

# Entanglement verification with detection-efficiency mismatch

Yanbao Zhang<sup>1,2</sup> and Norbert Lütkenhaus<sup>1,2</sup>

<sup>1</sup>*Institute for Quantum Computing, University of Waterloo, Waterloo, Ontario, N2L 3G1 Canada*

<sup>2</sup>*Department of Physics and Astronomy, University of Waterloo, Waterloo, Ontario, N2L 3G1 Canada*

(Dated: December 9, 2024)

The security analysis of quantum key distribution (QKD) is difficult to perform when there is efficiency mismatch between various threshold detectors involved in an experimental setup. Even the verification that the device actually performs in the quantum domain, referred to as the task of entanglement verification, is hard to perform. In this article we provide such an entanglement-verification method for characterized detection-efficiency mismatch. Our method does not rely on cut-off of photon numbers in the optical signal. It can be applied independently of the degrees of freedom involved, thus covering, for example, efficiency mismatch in polarization and time-bin modes, but also in spatial modes. The evaluation of typical experimental scenarios suggests that an increase of detection-efficiency mismatch will drive the performance of a given setup out of the quantum domain.

## I. Introduction

The ability to verify effective entanglement in observed data is a necessary condition for Alice and Bob to perform secure quantum key distribution (QKD) [1], demonstrate quantum teleportation [2] and realize quantum repeaters [3]. Many methods have been exploited for verifying entanglement. For example, one can apply the positive partial-transpose (PPT) criterion [4, 5], construct symmetric extensions of a quantum state [6], or build expectation-values matrices (EVMs) from experimental observations and apply corresponding entanglement criteria [7–11]. Also, one can verify entanglement by directly measuring special observables, e.g., Bell inequalities [12] or entanglement witnesses [13, 14]. (See the review paper [15] for a list and discussions of various methods.) For the typical QKD scenarios where Alice sends optical signals to Bob, we can model the underlying quantum state as Alice holding a discrete finite-dimensional system while Bob receiving an infinite-dimensional optical mode. In this case, EVM-based verification methods are particularly useful. They have been well developed [8, 10, 11, 16–18] and applied to real experiments [19, 20].

Almost all previously known methods for verifying entanglement assume that various threshold detectors involved in an experimental setup are ideal with perfect efficiency [34]. This assumption can be justified when there is no efficiency mismatch between these threshold detectors. In this case, one cannot distinguish no-detection events due to detection inefficiency from those due to transmission loss. For simplicity of analysis, one can lump these two kinds of loss together as a new increased transmission loss followed by ideal threshold detectors with perfect efficiency (see Sect. III C for detailed discussions about this treatment). Then, one can verify entanglement and further prove the security of the corresponding QKD protocols.

However, in practice it is hard to build two detectors that have exactly the same efficiency (for example, due

to different samples of the fabrication process). In the presence of efficiency mismatch, one cannot treat detection inefficiency in the same way as transmission loss, and so previously known methods cannot be applied for entanglement verification.

A detection-efficiency mismatch can also be induced by an adversary using the fact that a detector can respond to a photon differently depending on degrees of freedom (for example, spatial mode, frequency, or arriving time) other than those employed to encode information. If an adversary can control these degrees of freedom such that the induced efficiency mismatch is large enough, powerful attacks on QKD systems exist, as demonstrated in Refs. [21] and [22]. In typical experiments the efficiency mismatch may not seem significant, but it still means that the device cannot be covered by an existing security proof.

In this paper we develop a general method to verify entanglement in the presence of detection-efficiency mismatch. The method works as long as the efficiency mismatch is characterized, even if the mismatch depends on degrees of freedom of a photon that are not employed to encode information. We carefully study an implementation of the BB84-QKD prepare-and-measure protocol [23] with polarization encoding, where we take account of the fact that Bob receives signals in the infinite-dimensional mode space with no limit on the number of photons contained in that space. Our method is expected to work for other QKD protocols. The full security proof of QKD protocols with efficiency mismatch is still an open problem and is not addressed in the current paper either, though some essential tools developed here will carry over to such a security proof. Note that Ref. [24] studied the security proof of the BB84-QKD protocol with efficiency mismatch, under the additional assumption that Bob's system is a photonic qubit. However, this assumption is hard to justify in actual implementations of QKD where threshold detectors are being used.

The remainder of the paper is laid out as follows: In Sect. II, we describe an experimental setup for implementing the BB84-QKD protocol and the efficiency-

mismatch models considered. In Sect. III, we outline how our method works and explain details on how to apply the method to the particular experimental setup considered. In Sect. IV, we simulate experimental results according to a toy channel connecting Alice and Bob just for illustration purposes. For this toy channel, we present the bound on the efficiency mismatch in order for Alice and Bob to verify entanglement based only on their observations. Finally we conclude the paper in Sect. V.

## II. Experimental configuration

For simplicity, in this paper we consider an experimental implementation of the BB84-QKD prepare-and-measure protocol [23] with polarization encoding. In each run of the protocol, Alice prepares an optical signal where all the photons have the same polarization, randomly selected from the horizontal ( $H$ ), vertical ( $V$ ), diagonal ( $D$ ), or anti-diagonal ( $A$ ) polarizations. Then, Alice sends the optical signal to Bob, and Bob randomly selects to measure it either in the horizontal/vertical ( $H/V$ ) basis or the diagonal/anti-diagonal ( $D/A$ ) basis. After many runs of the protocol, if the final measurement results satisfy some conditions (for example, the quantum bit error rate is low enough), Alice and Bob can distill secret keys via some classical post-processing procedure. For the present study of entanglement verification, we only need to consider the quantum phase of the protocol, i.e., the above prepare-and-measure step.

Obviously, in the above implementation there is no entangled state physically shared between Alice and Bob. However, there is another equivalent description, i.e., the source-replacement description [1, 25], of the prepare-and-measure step in a general QKD protocol: In this thought setup, first Alice prepares an entangled state

$$|\Phi\rangle_{AA'} = \sum_{s=1}^S \sqrt{p_s} |s\rangle_A |\phi_s\rangle_{A'}, \quad (1)$$

where  $\{|s\rangle_A\}$  is a set of orthogonal states and  $p_s$  is the probability of preparing the signal state  $|\phi_s\rangle$ ,  $s = 1, 2, \dots, S$ . Second, Alice measures the system  $A$  with the projective positive-operator valued measure (POVM)  $\{|s\rangle\langle s|, s = 1, 2, \dots, S\}$ , and distributes the corresponding signal state  $|\phi_s\rangle$  to Bob. After the action of the channel (or Eve) on system  $A'$ , Bob receives a system  $B$  on which Bob performs a measurement. There is no way for Eve or any other party outside of Alice's lab to tell which description, either the prepare-and-measure or source-replacement description, is implemented at Alice's side. Entanglement between Alice's system  $A$  and Bob's system  $B$  (before their respective measurement) is required in the source-replacement description; otherwise, intercept-resend attacks on the QKD system exist. In this sense, we say that effective entanglement is a necessary condition for secure QKD [1].

To measure the polarization state of the incoming op-

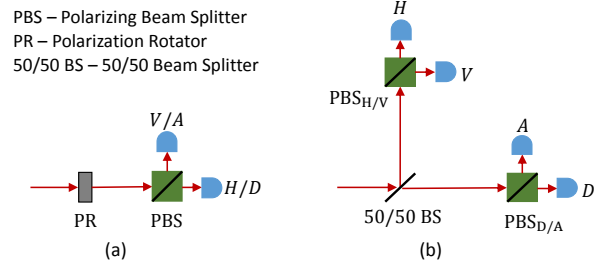


FIG. 1: Schematic of the measurement device: (a) is the active-detection scheme where a polarization rotator is used to select a measurement basis, and (b) is the passive-detection scheme where a 50/50 beam splitter is used to select a measurement basis. Under each basis, a polarizing beam splitter and two threshold detectors (which cannot distinguish the number of incoming photons) are used to measure the polarization state of photons. Each detector is labelled by the corresponding measurement outcome.

tical signal, Bob can employ either the active- or passive-detection scheme, as described in Fig. 1. The detectors involved in each detection scheme are threshold detectors which cannot distinguish the number of incoming photons. So, each detector has only two outcomes, click or no click. However, we do not restrict the number of photons arriving at each detector, due to the following two considerations: First, in practice information is usually encoded in coherent states which actually do have multi-photon components; second, the optical signal prepared by Alice can be intercepted by Eve and replaced by another stronger signal during the transmission from Alice to Bob.

In practice, the efficiencies of each detector will not be exactly the same. For the active-detection scheme as shown in Fig. 1(a), the detection efficiency is denoted by  $\eta_{H/D}$  if the measurement outcome is  $H$  or  $D$ , and the efficiency is denoted by  $\eta_{V/A}$  if the outcome is  $V$  or  $A$ . Similarly, for the passive-detection scheme as shown in Fig. 1(b), there are four detectors corresponding to the four measurement outcomes  $H$ ,  $V$ ,  $D$  and  $A$ . Denote their efficiencies by  $\eta_H$ ,  $\eta_V$ ,  $\eta_D$  and  $\eta_A$ . We will study entanglement verification in the presence of efficiency mismatch between these detectors. We call this the spatial-mode-independent mismatch model, in contrast to the following mismatch model where the mismatch depends additionally on the spatial modes.

As demonstrated in the recent works [26] and [27], not only differ the efficiencies of various detectors in a setup from each other, but also the efficiency mismatch depends on the spatial modes of incoming optical signals. As this kind of spatial-mode-dependent efficiency mismatch is quite relevant especially to implementations of free-space QKD, we would like to study the effect of this mismatch model on entanglement verification. In principle, the number of spatial modes of incoming optical signals can be arbitrary, even infinite. Intuitively, when the number of spatial modes is equal to or larger than

TABLE I: Spatial-mode-dependent mismatch model in the active-detection scheme, where  $0 \leq \eta \leq 1$ . Different columns are for different detectors labelled and shown in Fig. 1(a). Different rows are mismatched efficiencies for different spatial modes.

	Det. ‘H/D’	Det. ‘V/A’
Mode 1	1	$\eta$
Mode 2	$\eta$	1

TABLE II: Spatial-mode-dependent mismatch model in the passive-detection scheme, where  $0 \leq \eta \leq 1$ . Different columns are for different detectors labelled and shown in Fig. 1(b). Different rows are mismatched efficiencies for different spatial modes.

	Det. ‘H’	Det. ‘V’	Det. ‘D’	Det. ‘A’
Mode 1	1	$\eta$	$\eta$	$\eta$
Mode 2	$\eta$	1	$\eta$	$\eta$
Mode 3	$\eta$	$\eta$	1	$\eta$
Mode 4	$\eta$	$\eta$	$\eta$	1

the number of detectors in the measurement device, it might become possible for Eve to completely control Bob through the efficiency mismatch. For example, if each detector responds to an optical signal only in a particular spatial mode and different detectors respond to different spatial modes, then Eve can completely effectively switch on and off each detector by sending optical signals in these particular spatial modes. To illustrate the effect of spatial-mode-dependent efficiency mismatch on entanglement verification, we consider the case where the number of spatial modes is equal to the number of detectors. For illustration purposes, we also constrain the mismatch model so that mismatched efficiencies have a permutation symmetry over spatial modes. In particular, the mismatch models considered in the active- and passive-detection schemes are shown as in Tables I and II, respectively. According to the discussion in Sect. III C, we can renormalize detection efficiencies and treat the common loss in detectors as a part of transmission loss. Hence, we set the maximum detection efficiency in Table I or II to be 1. We would like to stress that we consider these mismatch models just for simplicity and ease of graphical illustrations: the method detailed in the next section works for general mismatch models.

### III. Our method

The main idea behind our method is to construct an expectation-values matrix (EVM) [8, 10, 11, 16–18] using a finite number of actual measurement operators which

contain efficiency-mismatch information. Let us discuss the construction and general properties of an EVM before moving on to our particular case.

Suppose that the joint system of Alice and Bob is described by a state  $\rho_{AB}$ , and that there are two sets of operators  $\{\hat{A}_i\}$  and  $\{\hat{B}_j\}$  acting on Alice’s and Bob’s subsystems, respectively. Then, the entries of an EVM  $\chi(\rho_{AB})$  are defined [35] as

$$[\chi(\rho_{AB})]_{ij,kl} = \text{Tr}(\rho_{AB} \hat{A}_i^\dagger \hat{A}_k \otimes \hat{B}_j^\dagger \hat{B}_l). \quad (2)$$

By the definition, several properties are satisfied by an EVM: First, an EVM is Hermitian and positive-semidefinite. Second, if both the sets of operators  $\{\hat{A}_i\}$  and  $\{\hat{B}_j\}$  are finite, the dimension of the EVM  $\chi(\rho_{AB})$  is finite even though the state  $\rho_{AB}$  is infinite dimensional. Third, entries of an EVM can be expectation values of observables, if the corresponding measurement operators are included in the set  $\{\hat{A}_i^\dagger \hat{A}_k \otimes \hat{B}_j^\dagger \hat{B}_l\}$ . Hence, an EVM will be designed as an object into which we can enter all experimental observations, but there may be undetermined entries. Still, we can study various properties, such as entanglement, of the underlying state. Fourth, the linear relationships between various operators  $\hat{A}_i^\dagger \hat{A}_k \otimes \hat{B}_j^\dagger \hat{B}_l$  restrict the entries  $\chi_{ij,kl}$ . (Here and later, we use  $\chi$  and  $\chi_{ij,kl}$  as short notations of  $\chi(\rho_{AB})$  and  $[\chi(\rho_{AB})]_{ij,kl}$  if there is no confusion in the context.) For example, if the operators satisfy

$$\sum_{ijkl} C_{ij,kl} \hat{A}_i^\dagger \hat{A}_k \otimes \hat{B}_j^\dagger \hat{B}_l \geq 0, \quad (3)$$

then for any density matrix  $\rho_{AB}$  the entries of the corresponding EVM satisfy

$$\sum_{ijkl} C_{ij,kl} \chi_{ij,kl} \geq 0, \quad (4)$$

where the coefficients  $C_{ij,kl}$  are complex numbers. Eq. (4) can be proved using the positivity of the whole operator in the left-hand side of Eq. (3) and the definition of an EVM. We will exploit all the above properties to reduce the number of free parameters in the constructed EVM and so reduce the complexity of the entanglement-verification problem.

Furthermore, to verify entanglement we need the following observation [10, 11]:

**Observation 1.** *If the state  $\rho_{AB}$  is separable, then  $\chi(\rho_{AB})$  has a separable structure and so satisfies the PPT criterion.*

This observation follows from the definition of an EVM and the PPT criterion [4, 5] satisfied by all separable (and even un-normalized) states. Note that an EVM is a un-normalized positive-semidefinite and Hermitian matrix. Thus, one can prove that the underlying state  $\rho_{AB}$  must be entangled by showing that the constructed EVM  $\chi$  cannot simultaneously satisfy the following two

constraints: First, the entries  $\chi_{ij,kl}$  are consistent with experimental observations and also with operator relationships; second,  $\chi \geq 0$  and  $\chi^{\Gamma_A} \geq 0$  where  $\Gamma_A$  is the partial-transpose operation on Alice's system. Hence, entanglement verification can be formulated as a semidefinite programming (SDP) problem which can be solved efficiently (see Sect. IIID for details).

To construct an EVM useful for our situation, we need to choose appropriate sets of operators  $\{\hat{A}_i\}$  and  $\{\hat{B}_j\}$ . In the following subsections, we will discuss in detail the set of operators that we consider in the case of efficiency mismatch, and also lay out several tricks that we can exploit to achieve our goal.

### A. Operators exploited for the construction of EVMs

Let us consider Alice's side first. Recall that, in the source-replacement description of a QKD protocol Alice first prepares the entangled state in Eq. (1) between systems  $A$  and  $A'$ . Subsequently, Alice measures the system  $A$  and sends the corresponding signal state encoded in system  $A'$  to Bob. In the above process, the system  $A$  remains at Alice. As a result, the reduced density matrix  $\rho_A$  of system  $A$  does not change even if the signal states change during the transmission from Alice to Bob. Also, Alice has complete knowledge of  $\rho_A$ , since the state in Eq. (1) is prepared and known by herself. Actually the overlap structure of signal states  $\{|\phi_s\rangle, s = 1, 2, \dots, S\}$  and the probabilities of preparing different signal states  $\{p_s, s = 1, 2, \dots, S\}$  determine the reduced state  $\rho_A$ . The rank of the density matrix  $\rho_A$  can be less than  $S$ , if the signal states prepared by Alice are linearly dependent. For example, in the ideal BB84-QKD protocol where information is encoded in the polarization of a single photon, the entangled state prepared by Alice is

$$|\Psi\rangle_{AA'} = \frac{1}{2}(|1\rangle_A |H\rangle_{A'} + |2\rangle_A |V\rangle_{A'} + |3\rangle_A |D\rangle_{A'} + |4\rangle_A |A\rangle_{A'}), \quad (5)$$

where  $|H\rangle, |V\rangle, |D\rangle$  and  $|A\rangle$  are single-photon states with horizontal, vertical, diagonal, and anti-diagonal polarizations, respectively. Although the reduced density matrix  $\rho_A$  is of dimension  $4 \times 4$ , it is easy to check that  $\rho_A$  lives in a 2-dimensional subspace and that Alice's measurement  $\{|1\rangle\langle 1|, |2\rangle\langle 2|, |3\rangle\langle 3|, |4\rangle\langle 4|\}$  also has a representation in the same 2-dimensional subspace.

To take advantage of the complete knowledge of Alice's state  $\rho_A$  and her measurement, we set the operators at Alice's side to be  $\hat{A}_i = |\phi\rangle\langle i|$  with  $i = 1, 2, \dots, n$ , where the pure states  $\{|i\rangle, i = 1, 2, \dots, n\}$  form a basis for the support of the density matrix  $\rho_A$  and  $|\phi\rangle$  is an arbitrary pure state of Alice's system. By choosing these operators, we can make sure that Alice's state and measurement results all are included in the constructed EVM (if the set of operators considered at Bob's side contains the

identity operator, which is usually a good choice).

Now, let us proceed to Bob's side. Depending on which detection scheme in Fig. 1 is used and which mismatch model is considered, the set of operators exploited is different. In the following subsection, we will discuss the operators exploited in the active-detection scheme with one spatial mode (i.e., the spatial-mode-independent scenario). The operators exploited in the other cases will be postponed to Appendix 1 due to their complexities.

#### 1. A basic construction of EVMs

In the active-detection scheme as shown in Fig. 1(a), the four possible events in a measurement basis are: click at only one of the two detectors (single click), clicks at both detectors (double click), and no click at neither of the two detectors. Suppose that the two detectors in Fig. 1(a) have efficiencies  $\eta_{H/D}$  and  $\eta_{D/A}$ , respectively. Then, the POVM elements for both the  $H/V$  and  $D/A$  measurement choices can be written down explicitly. For example, the POVM elements for the measurement in the  $H/V$  basis are

$$\begin{aligned} M_H &= \sum_{n_H=1}^{\infty} \sum_{n_V=0}^{\infty} (1 - (1 - \eta_{H/D})^{n_H}) (1 - \eta_{V/A})^{n_V} |n_H, n_V\rangle\langle n_H, n_V|, \\ M_V &= \sum_{n_H=0}^{\infty} \sum_{n_V=1}^{\infty} (1 - \eta_{H/D})^{n_H} (1 - (1 - \eta_{V/A})^{n_V}) |n_H, n_V\rangle\langle n_H, n_V|, \\ M_{HV} &= \sum_{n_H=1}^{\infty} \sum_{n_V=1}^{\infty} (1 - (1 - \eta_{H/D})^{n_H}) (1 - (1 - \eta_{V/A})^{n_V}) |n_H, n_V\rangle\langle n_H, n_V|, \text{ and} \\ M_{\emptyset}^+ &= \sum_{n_H=0}^{\infty} \sum_{n_V=0}^{\infty} (1 - \eta_{H/D})^{n_H} (1 - \eta_{V/A})^{n_V} |n_H, n_V\rangle\langle n_H, n_V|. \end{aligned} \quad (6)$$

Here, the subscripts of the POVM elements indicate the corresponding click events, the notation ' $\emptyset$ ' means no click, the superscript '+' denotes the  $H/V$  measurement basis, and  $|n_H, n_V\rangle$  is a photon-number basis state containing  $n_H$  horizontally polarized photons and  $n_V$  vertically polarized photons. See Appendix 2 for the derivation of the POVM elements in Eq. (6).

The POVM elements in Eq. (6) satisfy two properties. First, it is obvious to see that these POVM elements are diagonal in the photon-number basis  $\{|n_H, n_V\rangle, n_H, n_V = 0, 1, 2, \dots\}$ . Hence, any two of them commute. Second, because  $\eta_{H/D}$  and  $\eta_{V/A}$  are between 0 and 1, so are all coefficients of the terms  $|n_H, n_V\rangle\langle n_H, n_V|$  in Eq. (6). Hence, we get the following

relationships

$$M_i \geq M_i M_j \geq 0, \quad (7)$$

where  $i, j = H, V, HV$ , or  $\emptyset$ . Here, we write down  $A \geq B$  when  $(A - B)$  is a positive-semidefinite matrix. Using these two properties, we can restrict the entries of the constructed EVM if the measurement POVM elements in Eq. (6) are exploited.

The above two properties are also satisfied by the POVM elements for the measurement in the  $D/A$  basis. These POVM elements have the same expressions as those in Eq. (6) with the replacement of the subscripts  $H$  and  $V$  by  $D$  and  $A$ , respectively. For example, the POVM element for the single-click event with diagonal polarization is

$$M_D = \sum_{n_D=1}^{\infty} \sum_{n_A=0}^{\infty} (1 - (1 - \eta_{H/D})^{n_D}) (1 - \eta_{V/A})^{n_A} |n_D, n_A\rangle \langle n_D, n_A|, \quad (8)$$

where the basis state  $|n_D, n_A\rangle$  contains  $n_D$  diagonally polarized photons and  $n_A$  anti-diagonally polarized photons. The expressions of the other three POVM elements  $M_A, M_{DA}$  and  $M_{\emptyset}^{\times}$ , where the superscript ‘ $\times$ ’ indicates the  $D/A$  basis, can be found in Appendix 2.

The expectation values of the POVM elements for measurements in both the  $H/V$  and  $D/A$  bases are experimental observations. Therefore, in the construction of an EVM we can utilize these POVM elements. Since  $M_H + M_V + M_{HV} + M_{\emptyset}^+ = M_D + M_A + M_{DA} + M_{\emptyset}^{\times} = I$ , where  $I$  is the identity operator in the full state space, these POVM elements are not linearly independent. To construct an EVM, we will use the operators in the following linearly independent set

$$\mathcal{S} \equiv \{I, M_H, M_V, M_{HV}, M_D, M_A, M_{DA}\}. \quad (9)$$

Using the EVM constructed with the operators in the above set  $\mathcal{S}$ , we can verify entanglement when the observed error probability and observed double-click probability are low enough. To illustrate this result, in Sect. IV A we will study a particular channel connecting Alice and Bob. Then, it turns out that entanglement can be verified when the depolarizing probability  $\omega$  and the multi-photon probability  $p$  in the channel are low enough, as we will later see in Fig. 8.

## 2. An improved construction of EVMs

To improve the results, we consider projections of the operators in the set  $\mathcal{S}$  onto various photon-number subspaces. There are two reasons for exploiting these projections in the construction of an EVM: First, more operator relationships between these projections can be exploited. Second, as shown later, the expectation values of these projections can be bounded from experimental

observations. Both of these two help to constrain the constructed EVM. Generally speaking, the higher the number of considered photon-number subspaces, the stronger the entanglement-verification power of our method becomes. However, with increasing the number of considered photon-number subspaces the complexity of the resulting SDP problem increases.

For implementation simplicity, we consider the projections of operators onto the zero-photon, 1-photon, and 2-photons subspaces. The projections of the identity operator  $I$  onto those subspaces are denoted by  $I_{1 \times 1}$ ,  $I_{2 \times 2}$  and  $I_{3 \times 3}$ , respectively, where  $I_{d \times d}$  is the identity matrix of dimension  $d \times d$ . For the other operators in the set  $\mathcal{S}$ , from their explicit expressions (e.g., Eqs. (6) and (8)) we can see that their projections onto a photon-number subspace are linear combinations of ideal operators in the same subspace, where the combination coefficients depend on mismatched efficiencies. Here, the ideal operators are the projections of measurement POVM elements as setting all detection efficiencies to be perfect, and these ideal operators will be denoted by notations with tildes in order to be distinguished from real operators. For example, the projection of  $M_H$  in Eq. (6) onto the  $(\leq 2)$ -photons subspace  $M_H^{(\leq 2)}$  is

$$M_H^{(\leq 2)} = \eta_{H/D}(1 - \eta_{V/A})(I_{3 \times 3} - \tilde{M}_H^{(2)} - \tilde{M}_V^{(2)}) + (1 - (1 - \eta_{H/D})^2)\tilde{M}_H^{(2)} + \eta_{H/D}\tilde{M}_H^{(1)}, \quad (10)$$

where the superscript ‘(1)’ or ‘(2)’ means restriction to the 1-photon or 2-photons subspace. To write down all the projections, we need the following set of ideal operators

$$\{I_{1 \times 1}, I_{2 \times 2}, I_{3 \times 3}, \tilde{M}_H^{(1)}, \tilde{M}_D^{(1)}, \tilde{M}_H^{(2)}, \tilde{M}_V^{(2)}, \tilde{M}_D^{(2)}, \tilde{M}_A^{(2)}\}. \quad (11)$$

Note that we do not need the ideal operators  $\tilde{M}_V^{(1)}, \tilde{M}_A^{(1)}, \tilde{M}_{HV}^{(2)}$  and  $\tilde{M}_{DA}^{(2)}$ , due to the linear dependences  $\tilde{M}_H^{(1)} + \tilde{M}_V^{(1)} = \tilde{M}_D^{(1)} + \tilde{M}_A^{(1)} = I_{2 \times 2}$  and  $\tilde{M}_H^{(2)} + \tilde{M}_{HV}^{(2)} + \tilde{M}_V^{(2)} = \tilde{M}_D^{(2)} + \tilde{M}_{DA}^{(2)} + \tilde{M}_A^{(2)} = I_{3 \times 3}$ . Instead of the projections onto the  $(\leq 2)$ -photons subspace, we will use the ideal operators in Eq. (11) to construct an EVM, since the relationships between these ideal operators, as studied in Appendix 3, are simpler.

Moreover, there are relations between the ideal operators in Eq. (11) and measurement POVM elements. For example, because the POVM element  $M_H$  is block-diagonal with respect to various photon-number subspaces, we have that

$$M_H \geq M_H^{(\leq 2)}. \quad (12)$$

Then, considering Eq. (10), we can relate a linear combination of ideal operators in Eq. (11) to the measurement POVM element  $M_H$  by an inequality. Similar relations apply to other POVM elements. As a result, we can bound the expectation values of the ideal operators in Eq. (11) based on experimental observations. Therefore,

to construct an EVM, in addition to the operators in the set defined in Eq. (9) we can take advantage of the operators in the following sets

$$\mathcal{S}_0 \equiv \{|\text{Vac}\rangle \langle \text{Vac}|\}, \quad (13)$$

$$\mathcal{S}_1 \equiv \{I_{2 \times 2}, \tilde{M}_H^{(1)}, \tilde{M}_D^{(1)}, \sigma_y\}, \text{ and} \quad (14)$$

$$\mathcal{S}_2 \equiv \{I_{3 \times 3}, \tilde{M}_H^{(2)}, \tilde{M}_V^{(2)}, \tilde{M}_D^{(2)}, \tilde{M}_A^{(2)}, S_y\}. \quad (15)$$

Here,  $|\text{Vac}\rangle \langle \text{Vac}|$  is the projection onto the vacuum state  $|\text{Vac}\rangle$  (i.e., the zero-photon subspace), and the set  $\mathcal{S}_1$  or  $\mathcal{S}_2$  contains ideal operators in the 1-photon or 2-photons subspace, respectively. We include the qubit Pauli operator  $\sigma_y$  and the spin-1 operator  $S_y$  in the above sets, because they are involved in the commutation relationships between ideal operators (see Appendix 3). Note that any two operators from any two different sets as above are orthogonal to each other.

### B. Bounds on the number of photons arriving at Bob

In the previous subsection, we discussed several sets of ideal operators exploited for constructing an EVM. From experimental observations, we can bound expectation values of these ideal operators. Strictly speaking, we can bound their expectation values only from above (see Eq. (12) for an example). These upper-bound constraints can be satisfied in a trivial way, if the state does not lie in the same Hilbert space as the ideal operators exploited and so all expectation values of these ideal operators are zero. As a consequence, the relationships between these operators would not be helpful. Since we would like to exploit the operators particularly in the zero-photon, 1-photon, or 2-photons subspaces, we need to bound from below the probabilities that the state lies in these subspaces. In order to achieve this goal, we introduce additional constraints outside of the EVM formalism.

#### 1. Active-detection case

For the active-detection scheme we consider the following intuition: With the increase of the number of photons  $n$  arriving at Bob, the double-click probability (or the effective-error probability as defined below) conditional on the photon number  $n$  will increase and finally surpass the observed double-click probability (or the observed effective-error probability). Hence, in order to be consistent with experimental observations, the probability of a large number of photons arriving at Bob must be small. This motivates us to exploit the following double-click operator

$$F_{DC} = \frac{1}{2}I^A \otimes M_{HV}^B + \frac{1}{2}I^A \otimes M_{DA}^B, \quad (16)$$

and the effective-error operator

$$F_{EE} = \frac{1}{2}M_H^A \otimes (M_V^B + \frac{1}{2}M_{HV}^B) + \frac{1}{2}M_V^A \otimes (M_H^B + \frac{1}{2}M_{HV}^B) \\ + \frac{1}{2}M_D^A \otimes (M_A^B + \frac{1}{2}M_{DA}^B) + \frac{1}{2}M_A^A \otimes (M_D^B + \frac{1}{2}M_{DA}^B), \quad (17)$$

where the superscripts ‘A’ and ‘B’ denote Alice and Bob. The coefficient  $1/2$  before each term is due to the probability  $1/2$  of selecting the  $H/V$  or  $D/A$  measurement basis. According to the source-replacement description [25], Alice’s measurements  $M_H^A$ ,  $M_V^A$ ,  $M_D^A$  and  $M_A^A$  are ideal measurements in the 1-photon subspace. Bob’s measurement operators are as discussed in Sect. III A and Appendix 1a. Note that the definition of the above effective-error operator is motivated by the post-processing rule typically used in the squashing model [28, 29], where one randomly assigns a double-click event to one of the two single-click events at the same basis.

Before explaining how to utilize the operators  $F_{DC}$  and  $F_{EE}$ , let us discuss two properties of the state  $\rho_{AB}$  shared between Alice and Bob in the thought setup according to the source-replacement description. First, because measurement POVMs at Bob are block-diagonal with respect to various photon-number subspaces across all modes involved, we can assume without loss of generality that the state  $\rho_{AB}$  has the same block-diagonal structure. That is,  $\rho_{AB}$  can be written as

$$\rho_{AB} = \bigoplus_{n=0}^{\infty} p_n \rho_{AB}^{(n)}. \quad (18)$$

Here,  $p_n$  is the probability that the state  $\rho_{AB}$  lies in the  $n$ -photons subspace across all modes involved, and  $\rho_{AB}^{(n)}$  is the normalized state conditional on  $n$  photons arriving at Bob. Second, we can assume without loss of generality that  $\rho_{AB}$  and  $\rho_{AB}^{(n)}$  are real valued. This is because all measurement POVM elements  $M_x^A$  and  $M_y^B$  of Alice and Bob can be represented by real-valued matrices in the photon-number basis (see Ref. [8] for a detailed argument). The above two properties apply to the state  $\rho_{AB}$  under either the active- or passive-detection scheme. Considering the second property, we can reduce the number of free parameters in the constructed EVM and in the following optimization problems.

Now, let us proceed to formalize our intuition that the double-click probability (or the effective-error probability) conditional on the number of photons arriving at Bob increases with the photon number  $n$ . We study the

following optimization problems

$$\begin{aligned} d_{n,min} = & \min_{\rho_{AB}^{(n)}} d_n \\ \text{subject to } & \rho_{AB}^{(n)} \geq 0 \\ & \text{Tr}(\rho_{AB}^{(n)}) = 1 \\ & (\rho_{AB}^{(n)})^{\Gamma_A} \geq 0 \end{aligned} \quad (19)$$

and

$$\begin{aligned} e_{n,min} = & \min_{\rho_{AB}^{(n)}} e_n \\ \text{subject to } & \rho_{AB}^{(n)} \geq 0 \\ & \text{Tr}(\rho_{AB}^{(n)}) = 1 \\ & (\rho_{AB}^{(n)})^{\Gamma_A} \geq 0 \end{aligned} \quad (20)$$

where  $\Gamma_A$  is the partial-transpose operation on Alice's system, and the objective functions of the above two optimization problems are given by  $d_n = \text{Tr}(\rho_{AB}^{(n)} F_{DC}^{(n)})$  and  $e_n = \text{Tr}(\rho_{AB}^{(n)} F_{EE}^{(n)})$  respectively. The operators  $F_{DC}^{(n)}$  and  $F_{EE}^{(n)}$  are projections of the double-click operator  $F_{DC}$  and the effective-error operator  $F_{EE}$  onto the  $n$ -photons subspace of Bob. Note that in the above optimization problems we constrain the  $n$ -photons state  $\rho_{AB}^{(n)}$  such that its partial transpose is positive semidefinite. The reason is as follows: In order to verify entanglement we need to check whether or not there is a separable state consistent with experimental observations. Considering the block-diagonal structure of the state  $\rho_{AB}$ , if  $\rho_{AB}$  is separable then its projection onto any  $n$ -photons subspace  $\rho_{AB}^{(n)}$  must be separable and so satisfy the PPT criterion.

The optimization problems in Eqs. (19) and (20) are SDPs. We solved them numerically using the toolbox YALMIP [30] of MATLAB. We observed that, with the increase of the photon number  $n$ , both of the minimum double-click probability  $d_{n,min}$  and the minimum effective-error probability  $e_{n,min}$  monotonically increase and converge under an arbitrary mismatch model. (We have not proved this analytically, but numerical evidence strongly suggests that our observation is true.) The optimization results for the mismatch model specified in Table I are shown in Figs. 2 and 3. As a consequence, given the observed double-click probability  $d_{\text{obs}}$  and observed effective-error probability  $e_{\text{obs}}$ , we get that

$$d_{\text{obs}} = \sum_{n=0}^{\infty} p_n d_n \geq p_2 d_2 + (1 - p_0 - p_1 - p_2) d_{3,min}, \quad (21)$$

and

$$e_{\text{obs}} = \sum_{n=0}^{\infty} p_n e_n \geq p_1 e_1 + p_2 e_2 + (1 - p_0 - p_1 - p_2) e_{3,min}, \quad (22)$$

if the state  $\rho_{AB}$  is separable. Here, we use the facts that  $\sum_{n=0}^{\infty} p_n = 1$  and  $d_0 = d_1 = e_0 = 0$ . From the above two equations, obviously we get that  $d_{\text{obs}} \geq (1 - p_0 - p_1 - p_2) d_{3,min}$  and  $e_{\text{obs}} \geq (1 - p_0 - p_1 - p_2) e_{3,min}$ . Hence, we can bound from below the sum of the probabilities of zero photon, one photon and two photons ( $p_0 + p_1 + p_2$ ). Note that the parameters  $p_0, p_1, p_2, d_2, e_1$ , and  $e_2$  can be written as linear combinations of entries of the EVM, when the EVM is constructed with ideal operators in the ( $\leq 2$ )-photons subspace (as we implemented).

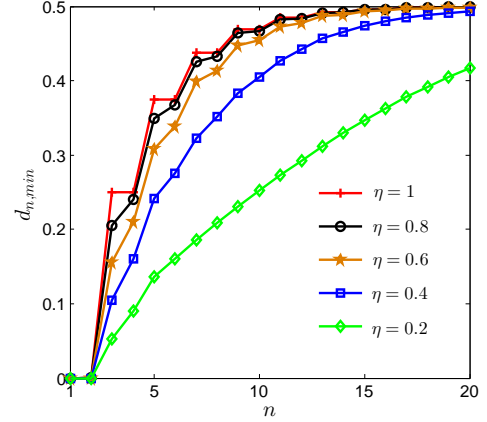


FIG. 2: The minimum double-click probability  $d_{n,min}$  as a function of the number of photons  $n$  arriving at Bob in the active-detection scheme. The results for the mismatch model specified in Table I are shown.

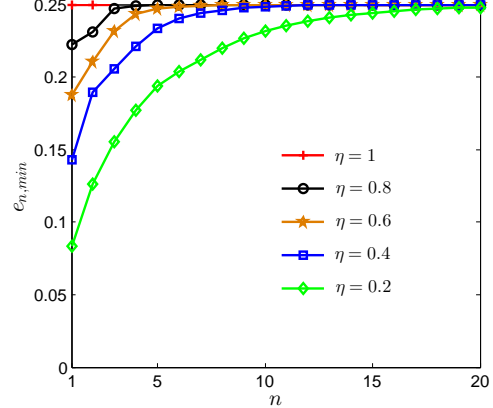


FIG. 3: The minimum effective-error probability  $e_{n,min}$  as a function of the number of photons  $n$  arriving at Bob in the active-detection scheme. The results for the mismatch model specified in Table I are shown.

## 2. Passive-detection case

In the passive-detection scheme as shown in Fig. 1(b), a 50/50 beam splitter is used for selecting different measurement bases. So, the probability that  $n$  incoming photons leave the beam splitter at different output arms is  $1 - 2^{-(n-1)}$ , which increases with the photon number  $n$ . These photons will potentially contribute to clicks at



two or more detectors at different output arms of the beam splitter, to which we refer as cross-click events. So, we expect that with the increase of  $n$  the cross-click probability conditional on  $n$  increases and converges to one. (In contrast, neither the double-click probability nor the effective-error probability increases with  $n$ , since the probability that  $n$  incoming photons leave the beam splitter at the same output arm decreases with  $n$ .) The above expectation motivates us to consider the following cross-click operator

$$F_{CC} = I^A \otimes M_{CC}^B, \quad (23)$$

where  $M_{CC}$  is the POVM element for cross-click events at Bob (see Appendix 1 b for details on the measurement POVM elements in the passive-detection scheme). Our expectation can be formalized as investigating the following optimization problem

$$\begin{aligned} c_{n,min} = & \min_{\rho_{AB}^{(n)}} c_n \\ \text{subject to } & \rho_{AB}^{(n)} \geq 0 \\ & \text{Tr}(\rho_{AB}^{(n)}) = 1 \\ & (\rho_{AB}^{(n)})^{\Gamma_A} \geq 0 \end{aligned} \quad (24)$$

where the objective function is given by  $c_n = \text{Tr}(\rho_{AB}^{(n)} F_{CC}^{(n)})$ , and  $F_{CC}^{(n)}$  is the projection of the cross-click operator  $F_{CC}$  onto the  $n$ -photons subspace of Bob. The same as in the active-detection case, we constrain the  $n$ -photons state  $\rho_{AB}^{(n)}$  such that it satisfies the PPT criterion.

The above optimization problem is a SDP, which can be solved numerically using the toolbox YALMIP [30] of MATLAB. Strong numerical evidence suggests that with the increase of  $n$  the minimum cross-click probability  $c_{n,min}$  monotonically increases and converges to one under an arbitrary mismatch model. For the mismatch model specified in Table II, the optimization results are shown in Fig. 4. As a result, given the observed cross-click probability  $c_{\text{obs}}$ , we have that

$$c_{\text{obs}} = \sum_{n=0}^{\infty} p_n c_n = \sum_{n=2}^{\infty} p_n c_n \geq (1 - p_0 - p_1) c_{2,min}. \quad (25)$$

Here, we use the facts that  $\sum_{n=0}^{\infty} p_n = 1$  and  $c_0 = c_1 = 0$ . Thus we can bound from below the probability of no more than one photon arriving at Bob.

In the end, we would like to make a comment on the effect of the detection-efficiency mismatch. From Figs. 2, 3 and 4, one can see that, given the photon number  $n$ , the larger the efficiency mismatch (i.e., the smaller the parameter  $\eta$ ), the smaller the minimum probability of induced double-click events, effective-error events, or cross-click events becomes. In this sense, we expect that the efficiency mismatch helps Eve to attack the QKD system.

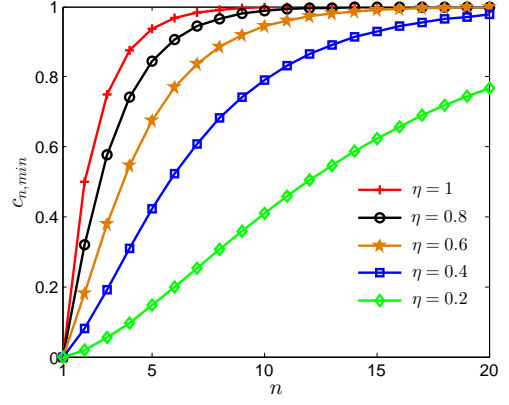


FIG. 4: The minimum cross-click probability  $c_{n,min}$  as a function of the number of photons  $n$  arriving at Bob in the passive-detection scheme. The results for the mismatch model specified in Table II are shown.

### C. Efficiency renormalization

The relative efficiencies of different detectors in Fig. 1 can be those described in Tables I and II. However, in practice no detector has an absolute efficiency 1. Suppose that the efficiencies of the two detectors in the active-detection scheme of Fig. 1(a) can be written as  $\eta_0\eta_1$  and  $\eta_0\eta_2$  respectively, where  $0 \leq \eta_0, \eta_1, \eta_2 \leq 1$ . Then, there are two equivalent descriptions of the same measurement device, as shown in Fig. 5. According to the description in Fig. 5(b), we can lump together the common loss  $\eta_0$  in the two detectors and the transmission loss in order to verify entanglement. The reason is as follows: Once entanglement is verified in the state shared between Alice and Bob after passing the beam splitter in Fig. 5(b), then the state before entering the whole measurement device in Fig. 5(a) must be entangled (otherwise, there is contradiction).

According to Fig. 5(b), the detection efficiencies  $\eta_{H/D}$  and  $\eta_{V/A}$  in measurement POVM elements, such as those in Eqs. (6) and (8), will be rescaled by a factor  $1/\eta_0$ . As we observed, given the photon number  $n$  arriving at Bob, with the increase of these detection efficiencies both the minimum double-click probability  $d_{n,min}$  and the minimum effective-error probability  $e_{n,min}$  increase. Hence, given experimental observations, by rescaling detection efficiencies the expectation values of ideal operators in the  $(\leq 2)$ -photons subspace can be bounded more tightly. We observed that more entangled states can be verified in this way than according to the description in Fig. 5(a). Therefore, in implementations of our method we renormalize detection efficiencies so that the maximum relative efficiency is 1. The same trick can be applied to the passive-detection scheme, as shown in Fig. 6. Note that the renormalization trick can also be applied to the case with multiple spatial modes. But, for this general case we need to renormalize the efficiencies over all detectors and over all spatial modes at the same time.



In a nutshell, our numerical observations show that if we renormalize detection efficiencies so that the maximum relative efficiency over all detectors and over all spatial modes is 1, then we can verify more entangled states than according to the actual description of the measurement device.

PR – Polarization Rotator    PBS – Polarizing Beam Splitter    BS – Beam Splitter

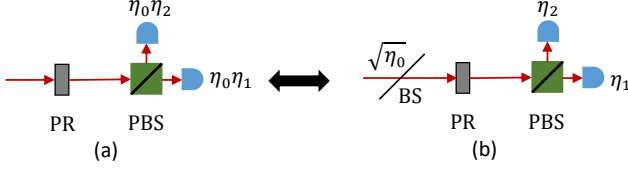


FIG. 5: Two equivalent descriptions of the same measurement device in the active-detection scheme, where the detection efficiency is written down around each detector and  $0 \leq \eta_0, \eta_1, \eta_2 \leq 1$ : (a) is the actual situation, and (b) is the hypothetical situation where the common loss  $\eta_0$  in the two detectors is factored out and treated as a part of transmission loss. The beam splitter in (b) has a transmission amplitude  $\sqrt{\eta_0}$ . See Appendix 4 for a proof of this equivalence.

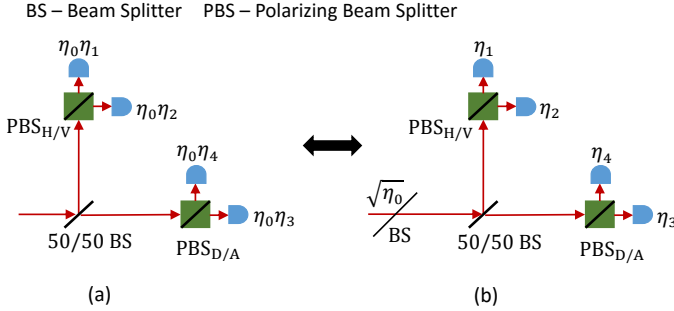


FIG. 6: Two equivalent descriptions of the same measurement device in the passive-detection scheme, where the detection efficiency is written down around each detector and  $0 \leq \eta_0, \eta_1, \eta_2, \eta_3, \eta_4 \leq 1$ : (a) is the actual situation, and (b) is the hypothetical situation where the common loss  $\eta_0$  in the four detectors is factored out and treated as a part of transmission loss. The first beam splitter in (b) has a transmission amplitude  $\sqrt{\eta_0}$ . See Appendix 5 for a proof of this equivalence.

#### D. SDP for entanglement verification

According to **Observation 1**, we can formulate entanglement verification as a SDP problem. Specifically, we need to solve a SDP feasibility problem of the form

$$\begin{aligned} & \text{find} && \chi \\ & \text{subject to} && \chi \geq 0 \text{ and } \chi^{\Gamma_A} \geq 0 \\ & && \sum_{ijkl} C_{ij,kl}^{(n)} \chi_{ij,kl} = 0, n = 1, 2, \dots, N \\ & && \sum_{ijkl} C_{ij,kl}^{(m)} \chi_{ij,kl} \geq 0, m = N + 1, 2, \dots, N + M \end{aligned} \quad (26)$$

Here, the matrix  $\chi$  is an EVM, the coefficients  $C_{ij,kl}^{(n)}$  with  $n = 1, 2, \dots, N + M$  are complex numbers, and  $N$  and  $M$  are the numbers of equality and inequality constraints respectively. The equality constraints are according to experimental observations and commutation relationships between operators (such as those in Eq. (56) of Appendix 3). The inequality constraints can be derived from operator relationships, such as those in Eqs. (7) and (12), or based on the inequalities in Eqs. (21), (22), and (25). If the SDP problem in Eq. (26) is not feasible, then the underlying state shared by Alice and Bob must be entangled. In our implementation, the optimization problem in Eq. (26) is solved using the toolbox YALMIP [30] of MATLAB.

#### IV. Demonstration with simulated results

The method discussed in Sect. III works for general detection-efficiency mismatch models. To illustrate our method, we consider particular mismatch models, such as those specified in Tables I and II. In the absence of a real experiment and for simplicity, we simulate experimental results according to a toy model detailed in the following subsection. We would like to stress that our method for verifying entanglement depends only on experimental observations and measurement POVMs but does not depend on the details of data simulation listed below.

##### A. Data simulation

We consider the ideal BB84-QKD protocol. Alice first prepares an entangled state as in Eq. (5) according to the source-replacement description. Then Alice sends out the polarized photon to Bob. We model the channel connecting Alice and Bob as a depolarizing channel with depolarizing probability  $\omega$ ; additionally, the transmission loss (i.e., the single-photon loss probability) over the channel is  $r$ ; and Eve intercepts the single photon and resends multiple photons to Bob with probability  $p$ . The multi-photon state resent by Eve is a randomly-polarized  $n$ -photons state of the form

$$\rho_n = \frac{1}{2n\pi} \int_0^{2\pi} d\theta \left( \hat{a}_\theta^\dagger \right)^n |0\rangle \langle 0| \left( \hat{a}_\theta \right)^n. \quad (27)$$

Here,  $\hat{a}_\theta^\dagger = \cos(\theta)\hat{a}_H^\dagger + \sin(\theta)\hat{a}_V^\dagger$ , and  $\hat{a}_H^\dagger$  (or  $\hat{a}_V^\dagger$ ) is the creation operator associated with the horizontally-polarized (or vertically-polarized) optical mode. The number of photons  $n$  resent will be specified later for each simulation. Moreover, when there is more than one spatial mode, the optical signal is distributed into each spatial mode uniformly randomly. For measurements at Bob, we consider both the active- and passive-detection schemes, as shown in Fig. 1.

### B. No-mismatch case and comparison with squashing models

When there is no efficiency mismatch between threshold detectors involved in the measurement device, one can verify entanglement based on squashing models [28, 29, 31, 32]. In this case, Bob uniformly randomly assigns a double-click event to one of the two single-click events at the same measurement basis, and assigns all cross-click events to no detection. Then, his observations can be thought of as generated by a qutrit system (constituted by a single photon and the vacuum). Once we can verify that this qutrit system is entangled with Alice's system, then the original system shared by Alice and Bob must be entangled [28, 31]. Note that it is still an open question whether or not a squashing model exists in the case of efficiency mismatch.

We compare our method with the one based on squashing models when there is no efficiency mismatch. For this purpose, we simulate experimental results according to the toy model specified in Sec. IV A. Particularly, we consider the case with no transmission loss. The comparison shows different behaviour, depending on the observations of Alice and Bob. To demonstrate the advantage of our method, we consider the case that the multi-photon state resent by Eve is of the form as in Eq. (27) with  $n = 2$ . (Note that the advantage of our method reduces with the increase of  $n$  and finally disappears.) To construct an EVM, we use both the measurement POVM elements (Eq. (9) for the active-detection scheme or Eq. (35) in Appendix 1 b for the passive-detection scheme) and the ideal operators in the  $(\leq 2)$ -photons subspace (Eqs. (13), (14) and (15)). The results in Fig. 7 demonstrate the advantage of our method for entanglement verification in the passive-detection scheme. This could be understood as follows: According to the squashing model we discard cross-click events, whereas in our method we take advantage of them in order to bound the number of photons arriving at Bob (see Eq. (25)). Fig. 7 also shows that when there is no mismatch the passive-detection scheme is better for verifying entanglement than the active-detection scheme. This is because the probability of detecting multi-photon events in the passive-detection scheme is higher than that in the active-detection scheme, given the same incoming multi-photon state. So, in the passive-detection scheme our method can take more advantage of operators in the  $(\leq 2)$ -photons subspace.

We also observe that it is useful to consider operators in various photon-number subspaces, as demonstrated in Fig. 8. In general, the higher the number of considered photon-number subspaces, the stronger the entanglement-verification power of our method becomes. But, with increasing the number of considered photon-number subspaces the complexity of the resulting SDP problem increases.

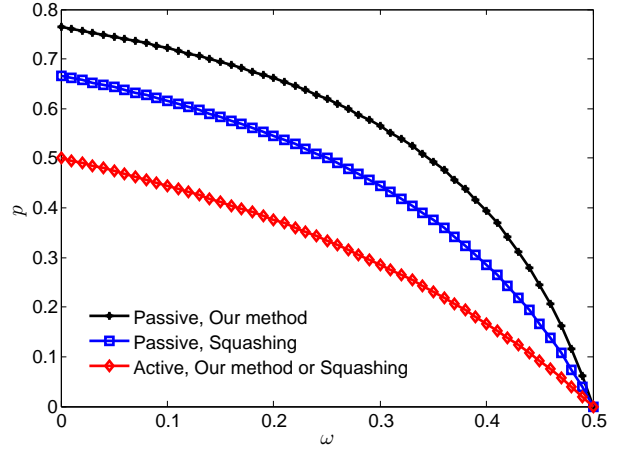


FIG. 7: Comparison of our method with the one based on squashing models when there is no efficiency mismatch and no transmission loss. Here,  $\omega$  is the depolarizing probability and  $p$  is the multi-photon probability in the channel. Below the curves entanglement can be verified. For the active-detection scheme, the results according to our method or based on squashing models coincide with each other, as shown in the red curve. For the passive-detection scheme, the results according to our method are shown in the black curve, whereas the results based on squashing models are shown in the blue curve.

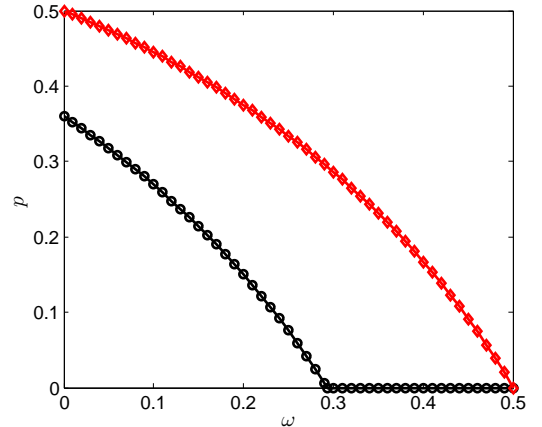


FIG. 8: Comparison of the results using EVMs constructed with different numbers of operators in the active-detection scheme. Here,  $\omega$  is the depolarizing probability and  $p$  is the multi-photon probability in the channel. Below the curves entanglement can be verified. The black curve shows the results when using only the measurement POVM elements (Eq. (9)) to construct an EVM, whereas the red curve shows the results when using both the measurement POVM elements (Eq. (9)) and the ideal operators in the  $(\leq 2)$ -photons subspace (Eqs. (13), (14) and (15)) to construct an EVM. Here, we consider the case with no efficiency mismatch and no transmission loss.

### C. Spatial-mode-independent mismatch

Let us start by considering the simple case where the efficiencies of various detectors involved can take different values, but the efficiencies are equal for every spatial

mode. To construct an EVM, we use both the measurement POVM elements (Eq. (9) for the active-detection scheme or Eq. (35) in Appendix 1b for the passive-detection scheme) and the ideal operators in the ( $\leq 2$ )-photons subspace (Eqs. (13), (14) and (15)). The results presented in this subsection are based on simulations according to the toy model specified in Sec. IV A. For simplicity, we assume that the multi-photon state resent by Eve is of the form as in Eq. (27) with  $n \rightarrow \infty$ .

First, we compare the abilities of verifying entanglement of the two detection schemes in Fig. 1, when efficiency mismatch is the same. Since there are two detectors in the active-detection scheme, up to permutation symmetry and efficiency renormalization as discussed in Sect. III C, there is only one kind of mismatch model. Hence, for the purpose of comparison, we consider the case  $\eta_{H/D} = 1$  and  $\eta_{V/A} = \eta < 1$  in the active-detection scheme, corresponding to the case  $\eta_H = \eta_D = 1$  and  $\eta_V = \eta_A = \eta < 1$  in the passive-detection scheme. We would like to find out the minimum efficiency  $\eta_{min}$  (corresponding to the maximum mismatch) such that entanglement can be verified as long as  $\eta \geq \eta_{min}$ . This minimum efficiency  $\eta_{min}$  characterizes the robustness of a detection scheme against mismatch for verifying entanglement. Typical results are shown in Fig. 9, where we fix the multi-photon probability  $p$  and the transmission loss  $r$ , and characterize the minimum efficiency  $\eta_{min}$  as a function of the depolarizing probability  $\omega$ . From Fig. 9, one can see that the minimum efficiencies in the active- and passive-detection schemes cross over with each other: For most values of  $\omega$  the active-detection scheme is better than the passive-detection scheme in terms of robustness against mismatch. However, there are regions for the values of  $\omega$  where the passive-detection scheme is better.

When there are no multi-photon events, i.e.,  $p = 0$ , our method can verify entanglement as long as the depolarizing probability satisfies  $\omega < 1/2$ , regardless of the values for the minimum efficiency  $\eta_{min}$  and transmission loss  $r$ . This is because when  $p = 0$  our method can certify that there is no more one photon arriving at Bob. Then, given the observed probability distribution and the mismatch model, the probability distribution for the no-mismatch case can be inferred. In the case of no mismatch, entanglement can be verified as long as the quantum bit error rate is less than 25% [33], which corresponds to the condition that the depolarizing probability satisfies  $\omega < 1/2$ .

Second, we study more general mismatch models in the passive-detection scheme. In this scheme, the efficiencies of the four detectors as shown in Fig. 1(b) can take different values from each other. When fixing the efficiencies of two of the four detectors, for example,  $\eta_H$  and  $\eta_D$ , there is a trade-off between the efficiencies of the other two detectors,  $\eta_V$  and  $\eta_A$ , in order to verify entanglement, as shown in Fig. 10.

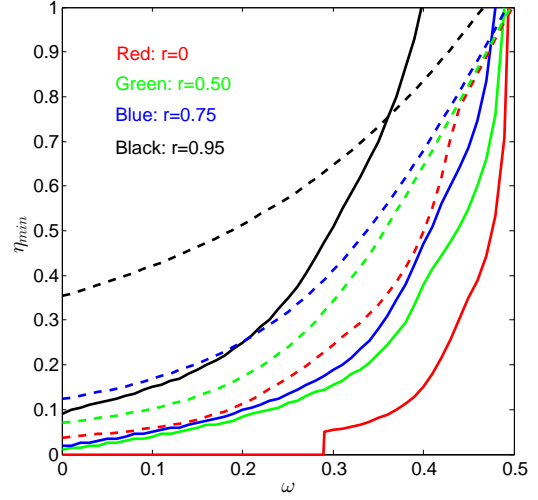


FIG. 9: Minimum efficiency  $\eta_{min}$  required for verifying entanglement as a function of the depolarizing probability  $\omega$  in the channel. The solid curves show the active-detection scheme, and the dash curves show the passive-detection scheme. Different colors are for different transmission losses  $r$  as labelled in the plot. Here, we fix the multi-photon probability  $p = 0.01$ . We choose the above values of  $r$  and  $p$  just for ease of graphical illustrations.

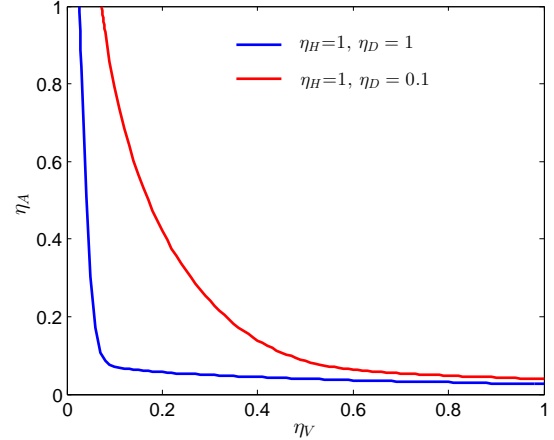


FIG. 10: Trade-off between efficiencies  $\eta_V$  and  $\eta_A$  under fixed values for  $\eta_H$  and  $\eta_D$  in the passive-detection scheme. When the point  $(\eta_V, \eta_A)$  is above the curve, entanglement can be verified by our method. Here, we fix the depolarizing probability  $\omega = 0.05$ , the multi-photon probability  $p = 0.01$ , and the transmission loss  $r = 0.5$ . We choose these values just for ease of graphical illustrations.

#### D. Spatial-mode-dependent mismatch

We now increase the number of spatial modes and consider spatial-mode-dependent mismatch models, such as those in Tables I and II. The results presented in this subsection are based on simulations according to the toy model specified in Sec. IV A. As in the previous subsection, we assume that the multi-photon state resent by Eve is of the form as in Eq. (27) with  $n \rightarrow \infty$ .

First, let us study the mismatch model in Table I for

the active-detection scheme. As in the previous subsection, we would like to find the minimum efficiency  $\eta_{min}$  characterizing the robustness of a detection scheme against mismatch for verifying entanglement. Here, we use both measurement POVM elements and the ideal operators in the  $(\leq 2)$ -photons subspace to construct an EVM (see Appendix 1a for details). When there is no transmission loss, i.e.,  $r = 0$ , the results are shown in Fig. 11. From this figure, one can see that the higher the depolarizing probability  $\omega$  or the multi-photon probability  $p$ , the larger the minimum efficiency  $\eta_{min}$  becomes for verifying entanglement. We also study the effect of transmission loss on entanglement verification, as shown in Fig. 12. From this figure, one can see that our method works well even for high-loss cases. The results in Figs. 11 and 12 suggest that the larger the efficiency mismatch (i.e., the smaller the efficiency  $\eta$ ), the smaller the set of noise parameters  $\omega$ ,  $p$  and  $r$  that preserve entanglement becomes.

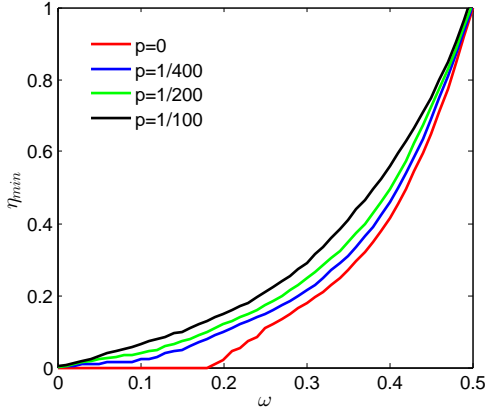


FIG. 11: Minimum efficiency  $\eta_{min}$  required for verifying entanglement as a function of the depolarizing probability  $\omega$  in the channel. Different colors are for different multi-photon probabilities  $p$  as labelled in the plot. Here we consider the active-detection scheme without transmission loss. The mismatch model studied is shown in Table I. We choose the above values of  $p$  just for ease of graphical illustrations.

Second, we study the mismatch model in Table II for the passive-detection scheme. Here, we use both measurement POVM elements and the ideal operators in the  $(\leq 1)$ -photon subspace to construct an EVM. Because of the implementation complexity, we do not consider the operators in the 2-photons subspace (see Appendix 1b for details). The results with or without transmission loss are shown in Figs. 13 and 14, respectively. These results also suggest that the larger the efficiency mismatch (i.e., the smaller the efficiency  $\eta$ ), the smaller the set of noise parameters  $\omega$ ,  $p$  and  $r$  that preserve entanglement becomes.

Note that we cannot compare the robustness of the two detection schemes against mismatch for verifying entanglement via Figs. 11 and 13 or via Figs. 12 and 14. The reasons are as follows: First, the mismatch models

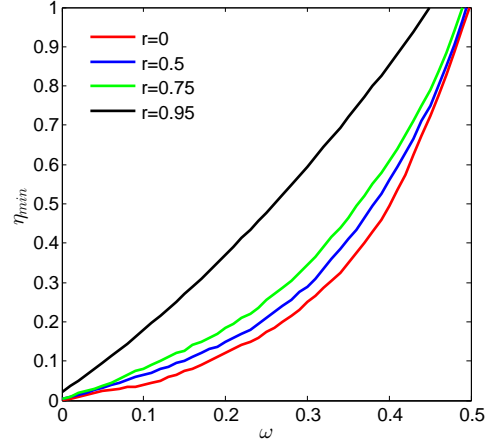


FIG. 12: Minimum efficiency  $\eta_{min}$  required for verifying entanglement as a function of the depolarizing probability  $\omega$  in the channel. Different colors are for different transmission losses  $r$  as labelled in the plot. Here we consider the active-detection scheme and fix the multi-photon probability  $p = 1/200$ . The mismatch model studied is shown in Table I. We choose the above values of  $r$  and  $p$  just for ease of graphical illustrations.

studied in Tables I and II, for the active- and passive-detection schemes respectively, are different. There is no one-to-one correspondence between these two mismatch models. Second, the EVMs for different detection schemes are constructed using different sets of operators. For the active-detection scheme we use the ideal operators in the  $(\leq 2)$ -photons subspace, whereas for the passive-detection scheme we use the ideal operators only in the  $(\leq 1)$ -photon subspace. The higher the number of considered photon-number subspaces, the stronger the entanglement-verification power of our method becomes. Hence, the comparison of the two detection schemes via Figs. 11 and 13 or via Figs. 12 and 14 would not be fair. We would like to stress that we have developed a general method for verifying entanglement with efficiency mismatch. How to optimize our method and improve its entanglement-verification power will require future study.

In the end, we would like to make two notes. First, numerical results suggest that when there are no multi-photon events the ability of our method to verify entanglement does not depend on transmission loss. (The results without multi-photon events and without transmission loss are shown in Figs. 11 and 13, for the active- and passive-detection schemes respectively.) Second, we studied the efficiency mismatch in the experiment of Ref. [26]. As Ref. [26] demonstrated, not only is efficiency mismatched between the four detectors used in the passive-detection scheme, but also the mismatch depends on which one of the four spatial modes contains the incoming optical signal. Ref. [26] studied two different cases, i.e., with or without a pinhole inserting in front of the measurement device. When there is no pinhole, the observed mismatch, as shown in Table III, is so large that successful intercept-resend attacks on the

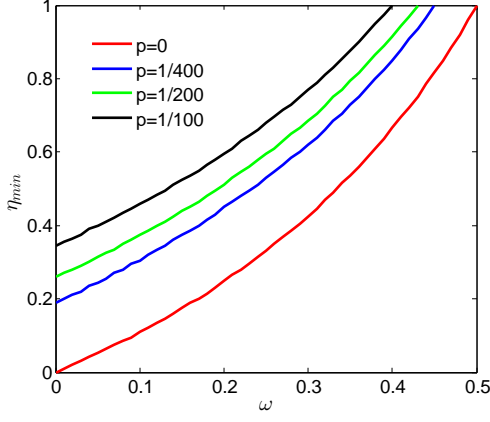


FIG. 13: Minimum efficiency  $\eta_{min}$  required for verifying entanglement as a function of the depolarizing probability  $\omega$  in the channel. Different colors are for different multi-photon probabilities  $p$  as labelled in the plot. Here we consider the passive-detection scheme without transmission loss. The mismatch model studied is shown in Table II. We choose the above values of  $p$  just for ease of graphical illustrations.

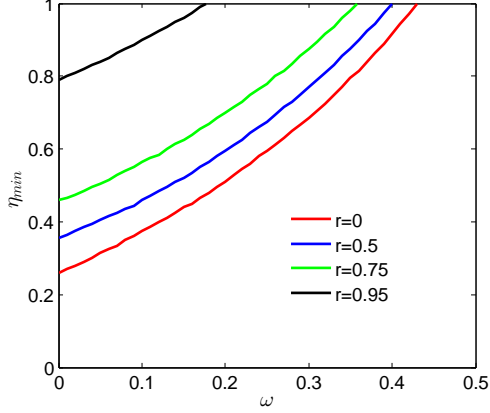


FIG. 14: Minimum efficiency  $\eta_{min}$  required for verifying entanglement as a function of the depolarizing probability  $\omega$  in the channel. Different colors are for different transmission losses  $r$  as labelled in the plot. Here we consider the passive-detection scheme and fix the multi-photon probability  $p = 1/200$ . The mismatch model studied is shown in Table II. We choose the above values of  $r$  and  $p$  just for ease of graphical illustrations.

QKD system exist. When there is a pinhole, the observed mismatch, as shown in Table IV, is reduced so that our method can verify entanglement.

## V. Conclusion

Many methods for verifying entanglement assume that various detectors involved in an experimental setup have the same efficiency and that the dimension of the quantum system is fixed and known. However, in practice, the efficiencies of detectors involved in a setup usually do

TABLE III: Spatial-mode-dependent mismatch observed in Ref. [26], when there is no pinhole. Different columns are for different detectors labelled and shown in Fig. 1(b). Different rows are mismatched efficiencies for different spatial modes.

	Det. 'H'	Det. 'V'	Det. 'D'	Det. 'A'
Mode 1	0.08	0	0.00106	0.00106
Mode 2	0	0.0008	0.0001	0.0001
Mode 3	0.002	0.002	0.16	0
Mode 4	0.002	0.002	0	0.04

TABLE IV: Spatial-mode-dependent mismatch observed in Ref. [26], when there is a pinhole. Different columns are for different detectors labelled and shown in Fig. 1(b). Different rows are mismatched efficiencies for different spatial modes.

	Det. 'H'	Det. 'V'	Det. 'D'	Det. 'A'
Mode 1	0.0004	0	0.0002	0.0002
Mode 2	0	0.0004	0.00033	0.00033
Mode 3	0.0002	0.0002	0.0004	0
Mode 4	0.00033	0.00033	0	0.0004

not take the same value, and the tested optical system is not well characterized. To address these problems, one can apply device-independent criteria, such as violations of Bell inequalities. However, these device-independent methods are not robust against transmission loss. Hence, they cannot verify many entangled states that appear in practice. Here, we present a method for verifying entanglement when the efficiency mismatch is characterized. Our method works without the knowledge of the system dimension. The method exploits relationships between measurement POVM elements, particularly those relationships between the projections of POVM elements onto the subspace that contains only a few of photons. The projections contain efficiency-mismatch information, and their expectation values are connected with experimental observations by inequalities. Hence, our method can take advantage of efficiency-mismatch information to verify entanglement.

We demonstrate our method with simulations. The results show that our method can verify entanglement even if there exists spatial-mode-dependent mismatch, which could be caused by an adversary in the QKD scenario. Moreover, our method is robust against transmission loss. For the no-mismatch case, there is another method for verifying entanglement based on squashing models [28, 29]. This method also does not require any system-dimension information. The simulation results show that our method can improve in some cases over squashing models (see Fig. 7). Moreover, it can verify entanglement even if the method using squashing models fails.



We have addressed the problem of verifying entanglement with efficiency mismatch even without knowing the dimension of the system. Future work is required to adapt the method to prove the security of QKD protocols with efficiency mismatch. It is also desirable to have an analytical proof of the monotonic behaviours of the double-click, effective-error, or cross-click probabilities as functions of the number of photons arriving at Bob, as demonstrated in Figs. 2, 3, and 4. These monotonic behaviours are important for taking advantage of operators in the subspace that contains only a few of photons.

### Acknowledgments

We thank Shihan Sajeed, Poompong Chaiwongkhot, and Vadim Makarov for useful discussions. We gratefully acknowledge supports through the Office of Naval Research (ONR), the Ontario Research Fund (ORF), the Natural Sciences and Engineering Research Council of Canada (NSERC), and Industry Canada.

### Appendix

#### 1. Operators exploited for constructing EVMs

In the main text, we discuss only the operators exploited in the case of the active-detection scheme with one spatial mode. Here, we will study other cases considered in the paper.

##### *a. Active-detection scheme with two spatial modes*

The idea behind constructing EVMs with two spatial modes (corresponding to the mismatch model in Table I) is the same as with one spatial mode studied in Sects. III A 1 and III A 2 of the main text. We consider both measurement POVM elements and ideal operators in the ( $\leq 2$ )-photons subspace for constructing an EVM. However, moving on to the two-spatial-modes case, measurement POVMs change their expressions. Also, more operators in the ( $\leq 2$ )-photons subspace can be exploited in order to construct an EVM. Let us discuss them in detail.

First, considering the tensor-product structure over the two spatial modes, POVM elements under a measurement setting change their expressions. For example, as long as there is a single-click event in one of the two spatial modes, it will contribute to the corresponding single-click event in experimental observations. So, the POVM elements for the single-click events under the  $H/V$  measurement setting are

$$M_{SC} = M_{SC,1} \otimes M_{\emptyset,2}^+ + M_{\emptyset,1}^+ \otimes M_{SC,2} + M_{SC,1} \otimes M_{SC,2}, \quad (28)$$

where the subscript ‘ $SC$ ’ can be either ‘ $H$ ’ or ‘ $V$ ’, and

the subscripts ‘1’ and ‘2’ index the two different spatial modes. For each spatial mode  $i$ ,  $i = 1, 2$ , the expressions of  $M_{H,i}$ ,  $M_{V,i}$  and  $M_{\emptyset,i}^+$  are the same as those in Eq. (6) with the replacement of  $\eta_{H/D}$  and  $\eta_{V/A}$  by  $\eta_{H/D,i}$  and  $\eta_{V/A,i}$ , the detection efficiencies in the spatial mode  $i$ . In a similar way, we can write down the other four POVM elements  $M_D$ ,  $M_A$ ,  $M_{HV}$  and  $M_{DA}$  required for constructing an EVM. Note that the measurement device cannot measure a photon in a basis that involves a superposition of different spatial modes. So, measurement POVM elements such as those in Eq. (28) are block-diagonal with respect to various photon-number subspaces where the number of photons in each spatial mode is specified.

Second, as for the one-spatial-mode case, the projections of POVM elements onto the zero-photon, 1-photon, or 2-photons subspaces are linear combinations of ideal operators in these subspaces. The operator set  $\mathcal{S}_0$  for the zero-photon subspace is still the same as in Eq. (13). For the 1-photon case, a photon can either lie in the spatial mode 1 or mode 2. So the set of ideal operators considered in Eq. (14) expands to two parallel sets

$$\mathcal{S}_{1,1} \equiv \{I_{2 \times 2,1}, \tilde{M}_{H,1}^{(1)}, \tilde{M}_{D,1}^{(1)}, \sigma_{y,1}\} \otimes |\text{Vac}\rangle_2 \langle \text{Vac}|, \quad (29)$$

and

$$\mathcal{S}_{1,2} \equiv |\text{Vac}\rangle_1 \langle \text{Vac}| \otimes \{I_{2 \times 2,2}, \tilde{M}_{H,2}^{(1)}, \tilde{M}_{D,2}^{(1)}, \sigma_{y,2}\}, \quad (30)$$

where the subscripts ‘1’ and ‘2’ denote the spatial mode 1 and 2, respectively. For each spatial mode  $i$ ,  $i = 1, 2$ , the ideal operators  $\tilde{M}_{H,i}^{(1)}$ ,  $\tilde{M}_{D,i}^{(1)}$  and  $\sigma_{y,i}$  are the same as those in Eqs. (11) and (52). For the 2-photons case, there are three possibilities: both photons are in the same mode 1 or 2, and one photon is in mode 1 and the other is in mode 2. For each of the first two possibilities, the set of ideal operators as defined in Eq. (15) becomes

$$\begin{aligned} \mathcal{S}_{2,1} \equiv & \{I_{3 \times 3,1}, \tilde{M}_{H,1}^{(2)}, \tilde{M}_{V,1}^{(2)}, \tilde{M}_{D,1}^{(2)}, \tilde{M}_{A,1}^{(2)}, S_{y,1}\} \\ & \otimes |\text{Vac}\rangle_2 \langle \text{Vac}|, \end{aligned} \quad (31)$$

or

$$\begin{aligned} \mathcal{S}_{2,2} \equiv & |\text{Vac}\rangle_1 \langle \text{Vac}| \otimes \\ & \{I_{3 \times 3,2}, \tilde{M}_{H,2}^{(2)}, \tilde{M}_{V,2}^{(2)}, \tilde{M}_{D,2}^{(2)}, \tilde{M}_{A,2}^{(2)}, S_{y,2}\}. \end{aligned} \quad (32)$$

The ideal operators in each spatial mode are the same as those in Eqs. (11) and (53). For the case that each spatial mode holds one photon, each mode is a qubit system and so the dimension of the whole space is  $2 \times 2 = 4$ . To describe the projections of measurement POVMs onto this subspace and their operator relationships, we need to consider the following set of ideal operators

$$\begin{aligned} \mathcal{S}_{2,1+2} \equiv & \{I_{2 \times 2,1} \otimes I_{2 \times 2,2}, \tilde{M}_{H,1}^{(1)} \otimes I_{2 \times 2,2}, \tilde{M}_{D,1}^{(1)} \otimes I_{2 \times 2,2}, \\ & \sigma_{y,1} \otimes I_{2 \times 2,2}, I_{2 \times 2,1} \otimes \tilde{M}_{H,2}^{(1)}, I_{2 \times 2,1} \otimes \tilde{M}_{D,2}^{(1)}, I_{2 \times 2,1} \otimes \sigma_{y,2}\}. \end{aligned} \quad (33)$$

Third, let us briefly discuss the relationships between operators within the sets  $\mathcal{S}$  (Eq. (9)),  $\mathcal{S}_{1,1}$  (Eq. (29)),  $\mathcal{S}_{1,2}$  (Eq. (30)),  $\mathcal{S}_{2,1}$  (Eq. (31)),  $\mathcal{S}_{2,2}$  (Eq. (32)), or  $\mathcal{S}_{2,1+2}$  (Eq. (33)). The relationships between operators in the set  $\mathcal{S}$  are the same as those discussed in the one-spatial-mode case. For each of the other operator sets, the relationships between operators can be derived from those between Pauli operators or between spin-1 operators (see Appendix 3). Moreover, any two operators from any two different sets of  $\mathcal{S}_{1,1}$ ,  $\mathcal{S}_{1,2}$ ,  $\mathcal{S}_{2,1}$ ,  $\mathcal{S}_{2,2}$  and  $\mathcal{S}_{2,1+2}$  are orthogonal to each other.

In the end, in order to exploit ideal operators within the sets  $\mathcal{S}_0$ ,  $\mathcal{S}_{1,1}$ ,  $\mathcal{S}_{1,2}$ ,  $\mathcal{S}_{2,1}$ ,  $\mathcal{S}_{2,2}$ , and  $\mathcal{S}_{2,1+2}$ , we need to know the relations between these ideal operators and measurement POVM elements. Once we know the relations, we can constrain expectation values of these ideal operators based on experimental observations. As in the one-spatial-mode case, the idea is to express the projections of measurement POVM elements onto the ( $\leq 2$ )-photons subspace as linear combinations of these ideal operators. Then, the relations are established.

#### b. Passive-detection case

In the passive-detection scheme as shown in Fig. 1(b), there are totally eight possible detection events: no click at any of the four detectors, click at only one of the four detectors (single click), clicks at two detectors at the same output arm of the beam splitter (double click), and clicks at two or more detectors at different output arms of the beam splitter (cross click).

Let us first consider the operators when there is only one spatial mode, since these operators are building blocks for more general cases. In contrast to the active-detection case, the explicit expressions of measurement POVM elements in the full state space are not easy to write out. Denote these POVM elements by  $M_\emptyset$ ,  $M_H$ ,  $M_V$ ,  $M_D$ ,  $M_A$ ,  $M_{HV}$ ,  $M_{DA}$ , and  $M_{CC}$ , where the subscripts indicate measurement outcomes and ‘CC’ means cross click. These operators are positive semidefinite and block-diagonal with respect to photon-number subspaces. Furthermore, since all POVM elements have eigenvalues between 0 and 1, they satisfy the following relationships

$$M_i \geq M_i M_i \geq 0, \quad (34)$$

where  $i$  can be  $\emptyset$ ,  $H$ ,  $V$ ,  $D$ ,  $A$ ,  $HV$ ,  $DA$ , or  $CC$ . Considering that  $M_\emptyset + M_H + M_V + M_D + M_A + M_{HV} + M_{DA} + M_{CC} = I$  where  $I$  is the identity operator in the full state space, we utilize the operator set

$$\mathcal{S} \equiv \{I, M_H, M_V, M_{HV}, M_D, M_A, M_{DA}, M_{CC}\}, \quad (35)$$

in order to construct an EVM.

We also consider the projections of the above POVM elements onto the ( $\leq 2$ )-photons subspace, and exploit relationships between these projections. As in the active-

detection case, these projections are linear combinations of ideal operators in the same subspace, where the combination coefficients depend on mismatched efficiencies (see Appendix 2 for more details). Also, we can bound the expectation values of these ideal operators. Hence, in addition to the operator set  $\mathcal{S}$  in Eq. (35) we also utilize the operator sets  $\mathcal{S}_0$ ,  $\mathcal{S}_1$  and  $\mathcal{S}_2$  in Eqs. (13), (14) and (15) for constructing an EVM.

Next, we consider the four-spatial-modes case (the corresponding mismatch model is shown in Table II). Considering the tensor-product structure over the four spatial modes, the no-click POVM element is

$$M_\emptyset = M_{\emptyset,1} \otimes M_{\emptyset,2} \otimes M_{\emptyset,3} \otimes M_{\emptyset,4}, \quad (36)$$

where the subscripts ‘1’, ‘2’, ‘3’ and ‘4’ are the indices of different spatial modes. Moreover, as long as there is a single click in one spatial mode, it will contribute to the observed single-click events. So the single-click POVM elements are

$$M_{SC} = M_{?,1} \otimes M_{?,2} \otimes M_{?,3} \otimes M_{?,4}, \quad (37)$$

where the subscript ‘SC’ means ‘H’, ‘V’, ‘D’ or ‘A’, and the notation ‘?’ can be either single click ‘SC’ or no detection ‘ $\emptyset$ ’ but at least one of  $M_{?,1}$ ,  $M_{?,2}$ ,  $M_{?,3}$  and  $M_{?,4}$  must be the single-click POVM element for the one-spatial-mode case. In a similar way, we can write down the expressions of  $M_{HV}$ ,  $M_{DA}$  and  $M_{CC}$ . Although measurement POVM elements change their forms, they still satisfy the relationships in Eq. (34).

To construct an EVM, we also consider the projections of measurement POVM elements onto the zero-photon and 1-photon subspaces. (Different from the one-spatial-mode case, we do not consider the projections onto the 2-photons subspace due to the complexity of both these operators and their relationships.) So, we need to consider ideal operators in the zero-photon and 1-photon subspaces. For the zero-photon case, we consider the operator set in Eq. (13). For the 1-photon case, we need to consider operator sets

$$\begin{aligned} \mathcal{S}_{1,1} \equiv & \{I_{2 \times 2,1}, \tilde{M}_{H,1}^{(1)}, \tilde{M}_{D,1}^{(1)}, \sigma_{y,1}\} \otimes |\text{Vac}\rangle_2 \langle \text{Vac}| \\ & \otimes |\text{Vac}\rangle_3 \langle \text{Vac}| \otimes |\text{Vac}\rangle_4 \langle \text{Vac}|, \end{aligned} \quad (38)$$

$$\begin{aligned} \mathcal{S}_{1,2} \equiv & |\text{Vac}\rangle_1 \langle \text{Vac}| \otimes \{I_{2 \times 2,2}, \tilde{M}_{H,2}^{(1)}, \tilde{M}_{D,2}^{(1)}, \sigma_{y,2}\} \\ & \otimes |\text{Vac}\rangle_3 \langle \text{Vac}| \otimes |\text{Vac}\rangle_4 \langle \text{Vac}|, \end{aligned} \quad (39)$$

$$\begin{aligned} \mathcal{S}_{1,3} \equiv & |\text{Vac}\rangle_1 \langle \text{Vac}| \otimes |\text{Vac}\rangle_2 \langle \text{Vac}| \\ & \otimes \{I_{2 \times 2,3}, \tilde{M}_{H,3}^{(1)}, \tilde{M}_{D,3}^{(1)}, \sigma_{y,3}\} \otimes |\text{Vac}\rangle_4 \langle \text{Vac}|, \end{aligned} \quad (40)$$

and

$$\begin{aligned} \mathcal{S}_{1,4} \equiv & |\text{Vac}\rangle_1 \langle \text{Vac}| \otimes |\text{Vac}\rangle_2 \langle \text{Vac}| \\ & \otimes |\text{Vac}\rangle_3 \langle \text{Vac}| \otimes \{I_{2 \times 2,4}, \tilde{M}_{H,4}^{(1)}, \tilde{M}_{D,4}^{(1)}, \sigma_{y,4}\}. \end{aligned} \quad (41)$$



The relationships between operators in each of the above sets can be derived from those between Pauli operators (see Appendix 3). And, the operators in different sets are orthogonal to each other. Moreover, these ideal operators are connected with measurement POVM elements by inequalities, so we can bound the expectation values of these ideal operators. In summary, for the four-spatial-modes case, we will utilize the operator sets in Eqs. (13), (35), (38), (39), (40) and (41) to construct an EVM.

## 2. POVM elements with mismatched efficiencies

We first consider the active-detection scheme as shown in Fig. 1(a). Suppose that the two threshold detectors have efficiencies  $\eta_{H/D}$  and  $\eta_{V/A}$ , respectively. Recall that a real threshold detector can be described by an ideal threshold detector with a beam splitter in front whose transmission amplitude is equal to the square root of the real detector's efficiency. It then turns out that the measurement in the  $H/V$  basis can be described by an optical device with three input spatial directions labelled by numbers and four output spatial directions labelled by lower-case letters, as shown in Fig. 15. In order to realize the measurement, however, only the input spatial direction 1 has incoming optical signals, whereas no signals travel along the other two input spatial directions 2 and 3. To get an outcome, the output modes  $H_a$  and  $V_c$  are measured with ideal threshold detectors, whereas the other two output modes  $H_b$  and  $V_d$  are not detected corresponding to the loss in the measurement process. (Note that here and later we use both the polarization degree of freedom and the spatial degree of freedom to label an input or output mode.) Therefore, it is straightforward to write down POVM elements in the output-modes basis  $\{|n_{H_a}, n_{H_b}, n_{V_c}, n_{V_d}\rangle, n_{H_a}, n_{H_b}, n_{V_c}, n_{V_d} = 0, 1, 2, \dots\}$ . For example, the POVM element for the single-click event 'H' is written as

$$M_H = \sum_{n_{H_a}=1}^{\infty} \sum_{n_{H_b}=0}^{\infty} \sum_{n_{V_d}=0}^{\infty} \frac{1}{n_{H_a}! n_{H_b}! n_{V_d}!} |n_{H_a}, n_{H_b}, 0_{V_c}, n_{V_d}\rangle \langle n_{H_a}, n_{H_b}, 0_{V_c}, n_{V_d}|. \quad (42)$$

Using the fact  $|n\rangle = \frac{1}{\sqrt{n!}}(\hat{a}^\dagger)^n |0\rangle$ , Eq. (42) becomes

$$M_H = \sum_{n_{H_a}=1}^{\infty} \sum_{n_{H_b}=0}^{\infty} \sum_{n_{V_d}=0}^{\infty} \frac{1}{n_{H_a}! n_{H_b}! n_{V_d}!} \left( \hat{a}_{H_a}^\dagger \right)^{n_{H_a}} \left( \hat{a}_{H_b}^\dagger \right)^{n_{H_b}} \left( \hat{a}_{V_d}^\dagger \right)^{n_{V_d}} |0\rangle \langle 0| \left( \hat{a}_{H_a} \right)^{n_{H_a}} \left( \hat{a}_{H_b} \right)^{n_{H_b}} \left( \hat{a}_{V_d} \right)^{n_{V_d}}, \quad (43)$$

where  $\hat{a}$  and  $\hat{a}^\dagger$  are annihilation and creation operators associated with an optical mode, respectively.

To express the POVM element  $M_H$  in the input-modes basis, we utilize the relations between creation operators

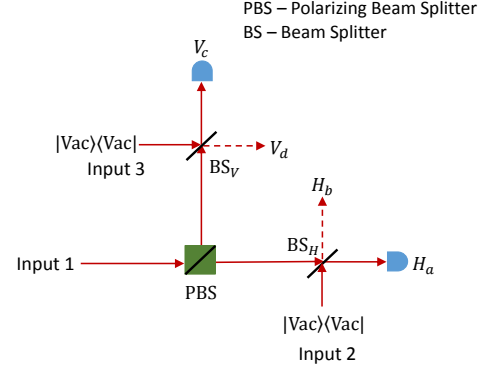


FIG. 15: Description of the measurement in the  $H/V$  basis under the active-detection scheme. Suppose that the detection efficiencies associated with the outcomes  $H$  and  $V$  are  $\eta_{H/D}$  and  $\eta_{V/A}$ , respectively, and that the two detectors shown are ideal. Then, the beam splitters BS<sub>H</sub> and BS<sub>V</sub> have transmission amplitudes  $\sqrt{\eta_{H/D}}$  and  $\sqrt{\eta_{V/A}}$ , respectively.

of the input and output modes of a beam splitter. Specifically, the relations

$$\begin{aligned} \hat{a}_{H_a}^\dagger &= \sqrt{\eta_{H/D}} \hat{a}_{H_1}^\dagger + \sqrt{1 - \eta_{H/D}} \hat{a}_{H_2}^\dagger, \\ \hat{a}_{H_b}^\dagger &= -\sqrt{1 - \eta_{H/D}} \hat{a}_{H_1}^\dagger + \sqrt{\eta_{H/D}} \hat{a}_{H_2}^\dagger, \text{ and} \\ \hat{a}_{V_d}^\dagger &= -\sqrt{1 - \eta_{V/A}} \hat{a}_{V_1}^\dagger + \sqrt{\eta_{V/A}} \hat{a}_{V_3}^\dagger. \end{aligned} \quad (44)$$

Using Eq. (44), we can express  $M_H$  in terms of the creation operators  $\hat{a}_{H_1}^\dagger, \hat{a}_{V_1}^\dagger, \hat{a}_{H_2}^\dagger$  and  $\hat{a}_{V_3}^\dagger$  and the annihilation operators  $\hat{a}_{H_1}, \hat{a}_{V_1}, \hat{a}_{H_2}$  and  $\hat{a}_{V_3}$ . Further, to fulfill the physical condition that there is no incoming optical signal travelling along the spatial directions 2 or 3, we need to pick only the terms where there is no appearance of any of the operators  $\hat{a}_{H_2}^\dagger, \hat{a}_{V_3}^\dagger, \hat{a}_{H_2}$ , and  $\hat{a}_{V_3}$ . Therefore, we get that

$$M_H = \sum_{n_{H_a}=1}^{\infty} \sum_{n_{H_b}=0}^{\infty} \sum_{n_{V_d}=0}^{\infty} \frac{1}{n_{H_a}! n_{H_b}! n_{V_d}!} (\eta_{H/D})^{n_{H_a}} (1 - \eta_{H/D})^{n_{H_b}} (1 - \eta_{V/A})^{n_{V_d}} \left( \hat{a}_{H_1}^\dagger \right)^{n_{H_a} + n_{H_b}} \left( \hat{a}_{V_1}^\dagger \right)^{n_{V_d}} |0\rangle \langle 0| \left( \hat{a}_{H_1} \right)^{n_{H_a} + n_{H_b}} \left( \hat{a}_{V_1} \right)^{n_{V_d}}. \quad (45)$$

Using the fact that  $(\hat{a}^\dagger)^n |0\rangle = \sqrt{n!} |n\rangle$ , and setting that  $n_{H_1} = n_{H_a} + n_{H_b}$  and  $n_{V_1} = n_{V_d}$ , we can simplify the above equation to

$$M_H = \sum_{n_{H_1}=1}^{\infty} \sum_{n_{V_1}=0}^{\infty} (1 - (1 - \eta_{H/D})^{n_{H_1}}) (1 - \eta_{V/A})^{n_{V_1}} |n_{H_1}, n_{V_1}\rangle \langle n_{H_1}, n_{V_1}|. \quad (46)$$

The above equation is the same as that in Eq. (6) of the main text, except that each polarization mode has a subscript '1' indicating the input spatial direction. Like-

wise, we can derive the other POVM elements for the measurement in the  $H/V$  basis, and the results are as follows:

$$\begin{aligned}
 M_V &= \sum_{n_{H_1}=0}^{\infty} \sum_{n_{V_1}=1}^{\infty} (1 - \eta_{H/D})^{n_{H_1}} (1 - (1 - \eta_{V/A})^{n_{V_1}}) \\
 &\quad |n_{H_1}, n_{V_1}\rangle \langle n_{H_1}, n_{V_1}|, \\
 M_{HV} &= \sum_{n_{H_1}=1}^{\infty} \sum_{n_{V_1}=1}^{\infty} (1 - (1 - \eta_{H/D})^{n_{H_1}}) (1 - (1 - \eta_{V/A})^{n_{V_1}}) \\
 &\quad |n_{H_1}, n_{V_1}\rangle \langle n_{H_1}, n_{V_1}|, \text{ and} \\
 M_{\emptyset}^+ &= \sum_{n_{H_1}=0}^{\infty} \sum_{n_{V_1}=0}^{\infty} (1 - \eta_{H/D})^{n_{H_1}} (1 - \eta_{V/A})^{n_{V_1}} \\
 &\quad |n_{H_1}, n_{V_1}\rangle \langle n_{H_1}, n_{V_1}|,
 \end{aligned} \tag{47}$$

where the superscript ‘+’ denotes the  $H/V$  basis.

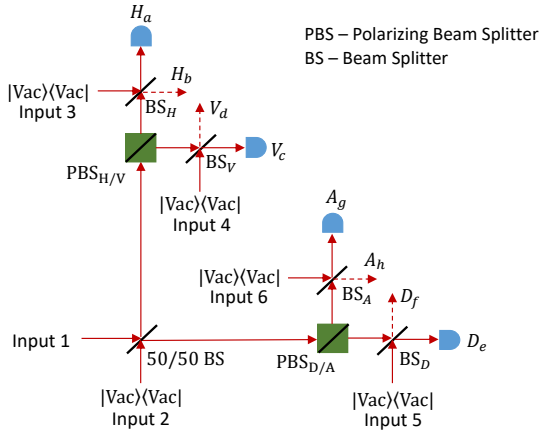


FIG. 16: Description of the measurement under the passive-detection scheme. Suppose that the detection efficiencies associated with the outcomes  $H$ ,  $V$ ,  $D$  and  $A$  are  $\eta_H$ ,  $\eta_V$ ,  $\eta_D$  and  $\eta_A$  respectively, and that the four detectors shown are ideal. Then, the beam splitters  $BS_H$ ,  $BS_V$ ,  $BS_D$  and  $BS_A$  have transmission amplitudes  $\sqrt{\eta_H}$ ,  $\sqrt{\eta_V}$ ,  $\sqrt{\eta_D}$  and  $\sqrt{\eta_A}$ , respectively.

We can follow the same procedure as above to derive the POVM elements for the measurement in the  $D/A$  basis under the active-detection scheme. We skip the details and just list the POVM elements as follows:

$$\begin{aligned}
 M_D &= \sum_{n_{D_1}=1}^{\infty} \sum_{n_{A_1}=0}^{\infty} (1 - (1 - \eta_{H/D})^{n_{D_1}}) (1 - \eta_{V/A})^{n_{A_1}} \\
 &\quad |n_{D_1}, n_{A_1}\rangle \langle n_{D_1}, n_{A_1}|,
 \end{aligned}$$

$$\begin{aligned}
 M_A &= \sum_{n_{D_1}=0}^{\infty} \sum_{n_{A_1}=1}^{\infty} (1 - \eta_{H/D})^{n_{D_1}} (1 - (1 - \eta_{V/A})^{n_{A_1}}) \\
 &\quad |n_{D_1}, n_{A_1}\rangle \langle n_{D_1}, n_{A_1}|, \\
 M_{DA} &= \sum_{n_{D_1}=1}^{\infty} \sum_{n_{A_1}=1}^{\infty} (1 - (1 - \eta_{H/D})^{n_{D_1}}) (1 - (1 - \eta_{V/A})^{n_{A_1}}) \\
 &\quad |n_{D_1}, n_{A_1}\rangle \langle n_{D_1}, n_{A_1}|, \text{ and} \\
 M_{\emptyset}^{\times} &= \sum_{n_{D_1}=0}^{\infty} \sum_{n_{A_1}=0}^{\infty} (1 - \eta_{H/D})^{n_{D_1}} (1 - \eta_{V/A})^{n_{A_1}} \\
 &\quad |n_{D_1}, n_{A_1}\rangle \langle n_{D_1}, n_{A_1}|.
 \end{aligned} \tag{48}$$

Here, the superscript ‘ $\times$ ’ denotes the  $D/A$  basis, and the subscript ‘1’ of the polarization mode denotes the input spatial direction.

Next, let us study the passive-detection case. With the help of the beam-splitter model for a real detector with imperfect efficiency, we can see that the whole measurement can be described by an optical device with six input spatial directions and eight output spatial directions, as shown in Fig. 16. To realize the measurement, only the input spatial direction 1 has incoming optical signals, and only the output modes  $H_a$ ,  $V_c$ ,  $D_e$  and  $A_g$  are measured (by ideal detectors). It is straightforward to see that, in the output-modes basis  $\{|n_{H_a}, n_{H_b}, n_{V_c}, n_{V_d}, n_{D_e}, n_{D_f}, n_{A_g}, n_{A_h}\rangle, |n_{H_a}, n_{H_b}, n_{V_c}, n_{V_d}, n_{D_e}, n_{D_f}, n_{A_g}, n_{A_h} = 0, 1, 2, \dots\rangle\}$ , the POVM element for the single-click event ‘ $H$ ’ is written as

$$\begin{aligned}
 M_H &= \sum_{n_{H_a}=1}^{\infty} \sum_{n_{H_b}=0}^{\infty} \sum_{n_{V_d}=0}^{\infty} \sum_{n_{D_f}=0}^{\infty} \sum_{n_{A_h}=0}^{\infty} \\
 &\quad |n_{H_a}, n_{H_b}, 0_{V_c}, n_{V_d}, 0_{D_e}, n_{D_f}, 0_{A_g}, n_{A_h}\rangle \\
 &\quad \langle n_{H_a}, n_{H_b}, 0_{V_c}, n_{V_d}, 0_{D_e}, n_{D_f}, 0_{A_g}, n_{A_h}|.
 \end{aligned} \tag{49}$$

To express the above POVM element  $M_H$  in the input-modes basis, as for the active-detection case, we use the fact that  $|n\rangle = \frac{1}{\sqrt{n!}} (\hat{a}^\dagger)^n |0\rangle$  and the relations between creation operators of the input and output modes of a beam splitter. Here, we omit the lengthy but not difficult details, and just write down the final expression of  $M_H$  as follows:

$$\begin{aligned}
 M_H &= \sum_{n_{H_a}=1}^{\infty} \sum_{n_{H_b}=0}^{\infty} \sum_{n_{V_d}=0}^{\infty} \sum_{n_{D_f}=0}^{\infty} \sum_{n_{A_h}=0}^{\infty} \\
 &\quad \left(\frac{1}{2}\right)^{n_{H_a}+n_{H_b}+n_{V_d}+n_{D_f}+n_{A_h}} \\
 &\quad \frac{1}{n_{H_a}! n_{H_b}! n_{V_d}! n_{D_f}! n_{A_h}!} (\eta_H)^{n_{H_a}} \\
 &\quad (1 - \eta_H)^{n_{H_b}} (1 - \eta_V)^{n_{V_d}} (1 - \eta_D)^{n_{D_f}} (1 - \eta_A)^{n_{A_h}} \\
 &\quad (\hat{a}_{H_1}^\dagger)^{n_{H_a}+n_{H_b}} (\hat{a}_{V_1}^\dagger)^{n_{V_d}} (\hat{a}_{D_1}^\dagger)^{n_{D_f}} (\hat{a}_{A_1}^\dagger)^{n_{A_h}}
 \end{aligned}$$

$$|0\rangle\langle 0| (\hat{a}_{H_1})^{n_{H_a}+n_{H_b}} (\hat{a}_{V_1})^{n_{V_d}} (\hat{a}_{D_1})^{n_{D_f}} (\hat{a}_{A_1})^{n_{A_h}}. \quad (50)$$

Likewise, we can get the following results

$$\begin{aligned}
M_V &= \sum_{n_{H_b}=0}^{\infty} \sum_{n_{V_c}=1}^{\infty} \sum_{n_{V_d}=0}^{\infty} \sum_{n_{D_f}=0}^{\infty} \sum_{n_{A_h}=0}^{\infty} \left(\frac{1}{2}\right)^{n_{H_b}+n_{V_c}+n_{V_d}+n_{D_f}+n_{A_h}} \\
&\quad \frac{1}{n_{H_b}! n_{V_c}! n_{V_d}! n_{D_f}! n_{A_h}!} (1-\eta_H)^{n_{H_b}} (\eta_V)^{n_{V_c}} (1-\eta_V)^{n_{V_d}} (1-\eta_D)^{n_{D_f}} (1-\eta_A)^{n_{A_h}} \\
&\quad \left(\hat{a}_{H_1}^\dagger\right)^{n_{H_b}} \left(\hat{a}_{V_1}^\dagger\right)^{n_{V_c}+n_{V_d}} \left(\hat{a}_{D_1}^\dagger\right)^{n_{D_f}} \left(\hat{a}_{A_1}^\dagger\right)^{n_{A_h}} |0\rangle\langle 0| (\hat{a}_{H_1})^{n_{H_b}} (\hat{a}_{V_1})^{n_{V_c}+n_{V_d}} (\hat{a}_{D_1})^{n_{D_f}} (\hat{a}_{A_1})^{n_{A_h}}, \\
M_D &= \sum_{n_{H_b}=0}^{\infty} \sum_{n_{V_d}=0}^{\infty} \sum_{n_{D_e}=1}^{\infty} \sum_{n_{D_f}=0}^{\infty} \sum_{n_{A_h}=0}^{\infty} \left(\frac{1}{2}\right)^{n_{H_b}+n_{V_d}+n_{D_e}+n_{D_f}+n_{A_h}} \\
&\quad \frac{1}{n_{H_b}! n_{V_d}! n_{D_e}! n_{D_f}! n_{A_h}!} (1-\eta_H)^{n_{H_b}} (1-\eta_V)^{n_{V_d}} (\eta_D)^{n_{D_e}} (1-\eta_D)^{n_{D_f}} (1-\eta_A)^{n_{A_h}} \\
&\quad \left(\hat{a}_{H_1}^\dagger\right)^{n_{H_b}} \left(\hat{a}_{V_1}^\dagger\right)^{n_{V_d}} \left(\hat{a}_{D_1}^\dagger\right)^{n_{D_e}+n_{D_f}} \left(\hat{a}_{A_1}^\dagger\right)^{n_{A_h}} |0\rangle\langle 0| (\hat{a}_{H_1})^{n_{H_b}} (\hat{a}_{V_1})^{n_{V_d}} (\hat{a}_{D_1})^{n_{D_e}+n_{D_f}} (\hat{a}_{A_1})^{n_{A_h}}, \\
M_A &= \sum_{n_{H_b}=0}^{\infty} \sum_{n_{V_d}=0}^{\infty} \sum_{n_{D_f}=0}^{\infty} \sum_{n_{A_g}=1}^{\infty} \sum_{n_{A_h}=0}^{\infty} \left(\frac{1}{2}\right)^{n_{H_b}+n_{V_d}+n_{D_f}+n_{A_g}+n_{A_h}} \\
&\quad \frac{1}{n_{H_b}! n_{V_d}! n_{D_f}! n_{A_g}! n_{A_h}!} (1-\eta_H)^{n_{H_b}} (1-\eta_V)^{n_{V_d}} (1-\eta_D)^{n_{D_f}} (\eta_A)^{n_{A_g}} (1-\eta_A)^{n_{A_h}} \\
&\quad \left(\hat{a}_{H_1}^\dagger\right)^{n_{H_b}} \left(\hat{a}_{V_1}^\dagger\right)^{n_{V_d}} \left(\hat{a}_{D_1}^\dagger\right)^{n_{D_f}} \left(\hat{a}_{A_1}^\dagger\right)^{n_{A_g}+n_{A_h}} |0\rangle\langle 0| (\hat{a}_{H_1})^{n_{H_b}} (\hat{a}_{V_1})^{n_{V_d}} (\hat{a}_{D_1})^{n_{D_f}} (\hat{a}_{A_1})^{n_{A_g}+n_{A_h}}, \\
M_{HV} &= \sum_{n_{H_a}=1}^{\infty} \sum_{n_{H_b}=0}^{\infty} \sum_{n_{V_c}=1}^{\infty} \sum_{n_{V_d}=0}^{\infty} \sum_{n_{D_f}=0}^{\infty} \sum_{n_{A_h}=0}^{\infty} \left(\frac{1}{2}\right)^{n_{H_a}+n_{H_b}+n_{V_c}+n_{V_d}+n_{D_f}+n_{A_h}} \\
&\quad \frac{1}{n_{H_a}! n_{H_b}! n_{V_c}! n_{V_d}! n_{D_f}! n_{A_h}!} (\eta_H)^{n_{H_a}} (1-\eta_H)^{n_{H_b}} (\eta_V)^{n_{V_c}} (1-\eta_V)^{n_{V_d}} (1-\eta_D)^{n_{D_f}} (1-\eta_A)^{n_{A_h}} \\
&\quad \left(\hat{a}_{H_1}^\dagger\right)^{n_{H_a}+n_{H_b}} \left(\hat{a}_{V_1}^\dagger\right)^{n_{V_c}+n_{V_d}} \left(\hat{a}_{D_1}^\dagger\right)^{n_{D_f}} \left(\hat{a}_{A_1}^\dagger\right)^{n_{A_h}} |0\rangle\langle 0| (\hat{a}_{H_1})^{n_{H_a}+n_{H_b}} (\hat{a}_{V_1})^{n_{V_c}+n_{V_d}} (\hat{a}_{D_1})^{n_{D_f}} (\hat{a}_{A_1})^{n_{A_h}}, \\
M_{DA} &= \sum_{n_{H_b}=0}^{\infty} \sum_{n_{V_d}=0}^{\infty} \sum_{n_{D_e}=1}^{\infty} \sum_{n_{D_f}=0}^{\infty} \sum_{n_{A_g}=1}^{\infty} \sum_{n_{A_h}=0}^{\infty} \left(\frac{1}{2}\right)^{n_{H_b}+n_{V_d}+n_{D_e}+n_{D_f}+n_{A_g}+n_{A_h}} \\
&\quad \frac{1}{n_{H_b}! n_{V_d}! n_{D_e}! n_{D_f}! n_{A_g}! n_{A_h}!} (1-\eta_H)^{n_{H_b}} (1-\eta_V)^{n_{V_d}} (\eta_D)^{n_{D_e}} (1-\eta_D)^{n_{D_f}} (\eta_A)^{n_{A_g}} (1-\eta_A)^{n_{A_h}} \\
&\quad \left(\hat{a}_{H_1}^\dagger\right)^{n_{H_b}} \left(\hat{a}_{V_1}^\dagger\right)^{n_{V_d}} \left(\hat{a}_{D_1}^\dagger\right)^{n_{D_e}+n_{D_f}} \left(\hat{a}_{A_1}^\dagger\right)^{n_{A_g}+n_{A_h}} |0\rangle\langle 0| (\hat{a}_{H_1})^{n_{H_b}} (\hat{a}_{V_1})^{n_{V_d}} (\hat{a}_{D_1})^{n_{D_e}+n_{D_f}} (\hat{a}_{A_1})^{n_{A_g}+n_{A_h}}, \\
&\quad \text{and} \\
M_\emptyset &= \sum_{n_{H_b}=0}^{\infty} \sum_{n_{V_d}=0}^{\infty} \sum_{n_{D_f}=0}^{\infty} \sum_{n_{A_h}=0}^{\infty} \left(\frac{1}{2}\right)^{n_{H_b}+n_{V_d}+n_{D_f}+n_{A_h}} \\
&\quad \frac{1}{n_{H_b}! n_{V_d}! n_{D_f}! n_{A_h}!} (1-\eta_H)^{n_{H_b}} (1-\eta_V)^{n_{V_d}} (1-\eta_D)^{n_{D_f}} (1-\eta_A)^{n_{A_h}} \left(\hat{a}_{H_1}^\dagger\right)^{n_{H_b}} \left(\hat{a}_{V_1}^\dagger\right)^{n_{V_d}} \\
&\quad \left(\hat{a}_{D_1}^\dagger\right)^{n_{D_f}} \left(\hat{a}_{A_1}^\dagger\right)^{n_{A_h}} |0\rangle\langle 0| (\hat{a}_{H_1})^{n_{H_b}} (\hat{a}_{V_1})^{n_{V_d}} (\hat{a}_{D_1})^{n_{D_f}} (\hat{a}_{A_1})^{n_{A_h}}. \quad (51)
\end{aligned}$$

It is not easy to simplify the expressions in Eqs. (50) and (51) further. But, from these expressions it is

straightforward to see that, the POVM elements are linear combinations of ideal operators where the combina-

tion coefficients are determined by the mismatched efficiencies  $\eta_H$ ,  $\eta_V$ ,  $\eta_D$  and  $\eta_A$ . Note that we did not write down the POVM element  $M_{CC}$  for cross-click events, since it can be inferred from the fact  $M_\emptyset + M_H + M_V + M_D + M_A + M_{HV} + M_{DA} + M_{CC} = I$  where  $I$  is the identity operator in the full state space.

### 3. Relationships between ideal operators

To figure out the relationships between the ideal operators in Eq. (11), we note that these ideal operators are related to Pauli operators (or spin- $\frac{1}{2}$  operators)

$$\sigma_x = \begin{pmatrix} 0 & 1 \\ 1 & 0 \end{pmatrix}, \sigma_y = \begin{pmatrix} 0 & -i \\ i & 0 \end{pmatrix}, \text{ and } \sigma_z = \begin{pmatrix} 1 & 0 \\ 0 & -1 \end{pmatrix}, \quad (52)$$

and spin-1 operators

$$S_x = \frac{1}{\sqrt{2}} \begin{pmatrix} 0 & 1 & 0 \\ 1 & 0 & 1 \\ 0 & 1 & 0 \end{pmatrix}, S_y = \frac{1}{\sqrt{2}} \begin{pmatrix} 0 & -i & 0 \\ i & 0 & -i \\ 0 & i & 0 \end{pmatrix}, \text{ and } S_z = \begin{pmatrix} 1 & 0 & 0 \\ 0 & 0 & 0 \\ 0 & 0 & -1 \end{pmatrix}. \quad (53)$$

Particularly, in the basis  $\{|1_H, 0_V\rangle, |0_H, 1_V\rangle\}$  of the 1-photon subspace we have

$$2\tilde{M}_H^{(1)} - I_{2 \times 2} = \sigma_z \text{ and } 2\tilde{M}_D^{(1)} - I_{2 \times 2} = \sigma_x, \quad (54)$$

and in the basis  $\{|2_H, 0_V\rangle, |1_H, 1_V\rangle, |0_H, 2_V\rangle\}$  of the 2-photons subspace we have

$$\tilde{M}_H^{(2)} - \tilde{M}_V^{(2)} = S_z \text{ and } \tilde{M}_D^{(2)} - \tilde{M}_A^{(2)} = S_x. \quad (55)$$

So, we can derive the relationships between the ideal operators in Eq. (11) from those between Pauli operators or between spin-1 operators, for example from,

$$\sigma_x \sigma_z = -i\sigma_y \text{ and } [S_x, S_z] = -iS_y. \quad (56)$$

### 4. Proof of the equivalence of descriptions in Fig. 5

Without loss of generality, we assume that the measurement is performed in the  $H/V$  basis. From Appendix 2, we already know the POVM elements for the measurement described in Fig. 5(a), i.e., Eqs. (46) and (47) with the replacement of  $\eta_{H/D}$  and  $\eta_{V/A}$  by  $\eta_0\eta_1$  and  $\eta_0\eta_2$ , respectively. To prove the equivalence, we can derive the POVM elements for the measurement described in Fig. 5(b). However, this approach is quite lengthy. To simplify the proof and make the idea behind clear, we take another approach. We study the transformation relations between the input creation operators and the output creation operators of the optical device in Fig. 5(a) or in Fig. 5(b). By inspecting these transforma-

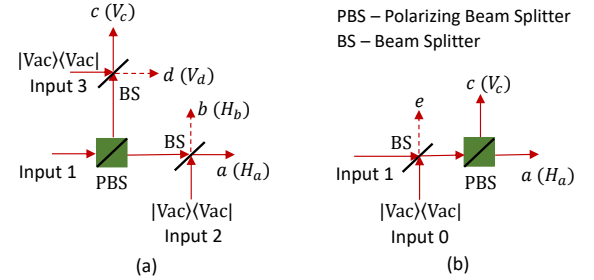


FIG. 17: Two equivalent descriptions of the measurement in the  $H/V$  basis under the active-detection scheme: (a) is the actual situation (the same as Fig. 5(a)), and (b) is the hypothetical situation (the same as Fig. 5(b)). Suppose that the detection efficiencies associated with the outcomes  $H$  and  $V$  can be written as  $\eta_0\eta_1$  and  $\eta_0\eta_2$  respectively, where  $0 \leq \eta_0, \eta_1, \eta_2 \leq 1$ . Then, to realize the measurement, each beam splitter as shown has a transmission amplitude  $\sqrt{\eta_0}$ , and the output modes  $H_a$  and  $V_c$  are detected with real detectors of efficiencies  $\eta_1$  and  $\eta_2$ , respectively. The two real detectors are not shown for simplicity. Note that the other output modes  $H_b$  and  $V_d$  in (a) and  $H_e$  and  $V_e$  in (b) are not detected, corresponding to the loss in the measurement process.

tion relations, we can prove the equivalence of Fig. 5(a) and Fig. 5(b).

It is straightforward to see that Fig. 5(a) (or Fig. 5(b)) is the same as Fig. 17(a) (or Fig. 17(b)) where only the input spatial direction 1 has incoming optical signals and only the output modes  $H_a$  and  $V_c$  are detected. For the optical device in Fig. 17(a), there are four input modes

$\{H_1, V_1, H_2, V_3\}$  and four output modes  $\{H_a, H_b, V_c, V_d\}$ . The transformation relations between the input and output modes can be easily derived from those between the

input and output modes of a beam splitter, such as those in Eq. (44). We skip the details and just write down the results as follows:

$$\begin{pmatrix} \hat{a}_{H_a}^\dagger \\ \hat{a}_{V_c}^\dagger \\ \hat{a}_{H_b}^\dagger \\ \hat{a}_{V_d}^\dagger \end{pmatrix} = \begin{pmatrix} \sqrt{\eta_0} & 0 & \sqrt{1-\eta_0} & 0 \\ 0 & \sqrt{\eta_0} & 0 & \sqrt{1-\eta_0} \\ -\sqrt{1-\eta_0} & 0 & \sqrt{\eta_0} & 0 \\ 0 & -\sqrt{1-\eta_0} & 0 & \sqrt{\eta_0} \end{pmatrix} \begin{pmatrix} \hat{a}_{H_1}^\dagger \\ \hat{a}_{V_1}^\dagger \\ \hat{a}_{H_2}^\dagger \\ \hat{a}_{V_3}^\dagger \end{pmatrix}. \quad (57)$$

We denote the above transformation matrix by  $T$ .

For the optical device in Fig. 17(b), there are also four input modes  $\{H_1, V_1, H_0, V_0\}$  and four output modes

$\{H_a, V_c, H_e, V_e\}$ . The input creation operators and the output creation operators are related by

$$\begin{pmatrix} \hat{a}_{H_a}^\dagger \\ \hat{a}_{V_c}^\dagger \\ \hat{a}_{H_e}^\dagger \\ \hat{a}_{V_e}^\dagger \end{pmatrix} = \begin{pmatrix} \sqrt{\eta_0} & 0 & \sqrt{1-\eta_0} & 0 \\ 0 & \sqrt{\eta_0} & 0 & \sqrt{1-\eta_0} \\ -\sqrt{1-\eta_0} & 0 & \sqrt{\eta_0} & 0 \\ 0 & -\sqrt{1-\eta_0} & 0 & \sqrt{\eta_0} \end{pmatrix} \begin{pmatrix} \hat{a}_{H_1}^\dagger \\ \hat{a}_{V_1}^\dagger \\ \hat{a}_{H_0}^\dagger \\ \hat{a}_{V_0}^\dagger \end{pmatrix}. \quad (58)$$

We denote the above transformation matrix by  $T'$ .

If we replace the input modes  $H_2$  and  $V_3$  by  $H_0$  and  $V_0$  and replace the output modes  $H_b$  and  $V_d$  by  $H_e$  and  $V_e$ , we can see that the transformation matrix  $T$  in Eq. (57) becomes  $T'$  in Eq. (58). Since neither the input modes  $H_2$  and  $V_3$  in Fig. 17(a) nor  $H_0$  and  $V_0$  in Fig. 17(b) have incoming optical signals, and neither the output modes  $H_b$  and  $V_d$  in Fig. 17(a) nor  $H_e$  and  $V_e$  in Fig. 17(b) are detected, we conclude that the two optical devices in Fig. 17(a) and Fig. 17(b) are equivalent. Hence, the two descriptions of the measurement in the active-detection scheme as in Fig. 5(a) and Fig. 5(b) are equivalent.

## 5. Proof of the equivalence of descriptions in Fig. 6

In the passive-detection scheme as shown in Fig. 1(b), each output arm of the 50/50 beam splitter is a setup for the active-detection scheme, i.e., a polarizing beam splitter with two detectors in both output arms of the polarizing beam splitter. From Fig. 17 of Appendix 4, we already see that the common loss in the two output arms of a polarizing beam splitter can be introduced either by inserting a beam splitter in each output arm or by inserting a beam splitter with the same transmission amplitude in the input arm of the polarizing beam splitter. Hence, to prove the equivalence of Fig. 6(a) and Fig. 6(b), we only need to further prove that the com-

mon loss in the two output arms of a 50/50 beam splitter is equivalent to the common loss in the two input arms of the 50/50 beam splitter, as shown in Fig. 18.

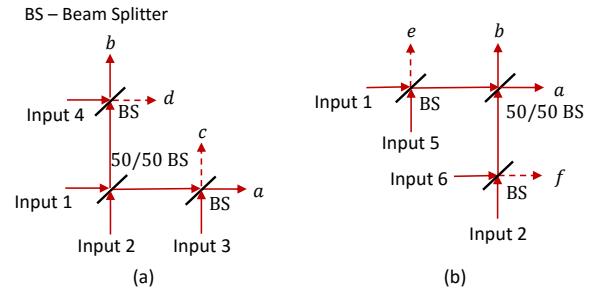


FIG. 18: Two equivalent descriptions of a 50/50 beam splitter with losses: (a) is the case where the loss is introduced in each output arm, and (b) is the case where the loss is introduced in each input arm. Suppose that the common loss factor is  $\eta_0$ . Then, each beam splitter BS as shown has a transmission amplitude  $\sqrt{\eta_0}$ . The whole optical device in each case has four input spatial directions and four output spatial directions.

To prove the equivalence of Fig. 18(a) and Fig. 18(b), we study the transformation relations between the input creation operators and the output creation operators for each case. It is straightforward to get that the transmission matrix  $T$  for the device in Fig. 18(a) is given by

$$\begin{pmatrix} \hat{a}_a^\dagger \\ \hat{a}_b^\dagger \\ \hat{a}_c^\dagger \\ \hat{a}_d^\dagger \end{pmatrix} = \begin{pmatrix} \sqrt{\eta_0/2} & \sqrt{\eta_0/2} & \sqrt{1-\eta_0} & 0 \\ -\sqrt{\eta_0/2} & \sqrt{\eta_0/2} & 0 & \sqrt{1-\eta_0} \\ -\sqrt{(1-\eta_0)/2} & -\sqrt{(1-\eta_0)/2} & \sqrt{\eta_0} & 0 \\ \sqrt{(1-\eta_0)/2} & -\sqrt{(1-\eta_0)/2} & 0 & \sqrt{\eta_0} \end{pmatrix} \begin{pmatrix} \hat{a}_1^\dagger \\ \hat{a}_2^\dagger \\ \hat{a}_3^\dagger \\ \hat{a}_4^\dagger \end{pmatrix}. \quad (59)$$

The transmission matrix  $T'$  for the device in Fig. 18(b) is given by

$$\begin{pmatrix} \hat{a}_a^\dagger \\ \hat{a}_b^\dagger \\ \hat{a}_e^\dagger \\ \hat{a}_f^\dagger \end{pmatrix} = \begin{pmatrix} \sqrt{\eta_0/2} & \sqrt{\eta_0/2} & \sqrt{(1-\eta_0)/2} & -\sqrt{(1-\eta_0)/2} \\ -\sqrt{\eta_0/2} & \sqrt{\eta_0/2} & -\sqrt{(1-\eta_0)/2} & -\sqrt{(1-\eta_0)/2} \\ -\sqrt{1-\eta_0} & 0 & \sqrt{\eta_0} & 0 \\ 0 & \sqrt{1-\eta_0} & 0 & \sqrt{\eta_0} \end{pmatrix} \begin{pmatrix} \hat{a}_1^\dagger \\ \hat{a}_2^\dagger \\ \hat{a}_5^\dagger \\ \hat{a}_6^\dagger \end{pmatrix}. \quad (60)$$

At first sight, the two transmission matrices  $T$  and  $T'$  are not the same. However, if we redefine the creation operators  $\hat{a}_5^\dagger = (\hat{a}_5^\dagger - \hat{a}_6^\dagger)/\sqrt{2}$ ,  $\hat{a}_6^\dagger = -(\hat{a}_5^\dagger + \hat{a}_6^\dagger)/\sqrt{2}$ ,  $\hat{a}_e^\dagger = (\hat{a}_e^\dagger - \hat{a}_f^\dagger)/\sqrt{2}$ , and  $\hat{a}_f^\dagger = -(\hat{a}_e^\dagger + \hat{a}_f^\dagger)/\sqrt{2}$ , then the transmission matrix  $T'$  becomes  $T$  by relabelling the input and output spatial directions. Since neither the input spatial directions 3 and 4 in Fig. 18(a) nor 5 and 6 in

Fig. 18(b) have incoming optical signals, and neither the output spatial directions  $c$  and  $d$  in Fig. 18(a) nor  $e$  and  $f$  in Fig. 18(b) are detected, we conclude that the two optical devices in Fig. 18(a) and Fig. 18(b) are equivalent. Hence, the two descriptions of the measurement in the passive-detection scheme as in Fig. 6(a) and Fig. 6(b) are equivalent.

- 
- [1] M. Curty, M. Lewenstein, and N. Lütkenhaus, Phys. Rev. Lett. **92**, 217903 (2004).
  - [2] C. H. Bennett, G. Brassard, C. Crépeau, R. Jozsa, A. Peres, and W. K. Wootters, Phys. Rev. Lett. **70**, 1895 (1993), URL <http://link.aps.org/doi/10.1103/PhysRevLett.70.1895>.
  - [3] H.-J. Briegel, W. Dür, J. I. Cirac, and P. Zoller, Phys. Rev. Lett. **81**, 5932 (1998), URL <http://link.aps.org/doi/10.1103/PhysRevLett.81.5932>.
  - [4] A. Peres, Phys. Rev. Lett. **77**, 1413 (1996), URL <http://link.aps.org/doi/10.1103/PhysRevLett.77.1413>.
  - [5] M. Horodecki, P. Horodecki, and R. Horodecki, Phys. Lett. A **223**, 1 (1996).
  - [6] A. C. Doherty, P. A. Parrilo, and F. M. Spedalieri, Phys. Rev. Lett. **88**, 187904 (2002), URL <http://link.aps.org/doi/10.1103/PhysRevLett.88.187904>.
  - [7] E. Shchukin and W. Vogel, Phys. Rev. Lett. **95**, 230502 (2005), URL <http://link.aps.org/doi/10.1103/PhysRevLett.95.230502>.
  - [8] J. Rigas, O. Gühne, and N. Lütkenhaus, Phys. Rev. A **73**, 012341 (2006), URL <http://link.aps.org/doi/10.1103/PhysRevA.73.012341>.
  - [9] M. Navascués, S. Pironio, and A. Acín, Phys. Rev. Lett. **98**, 010401 (2007).
  - [10] H. Häsele, T. Moroder, and N. Lütkenhaus, Phys. Rev. A **77**, 032303 (2008), URL <http://link.aps.org/doi/10.1103/PhysRevA.77.032303>.
  - [11] T. Moroder, J.-D. Bancal, Y.-C. Liang, M. Hofmann, and O. Gühne, Phys. Rev. Lett. **111**, 030501 (2013), URL <http://link.aps.org/doi/10.1103/PhysRevLett.111.030501>.
  - [12] J. S. Bell, Physics **1**, 195 (1964).
  - [13] B. M. Terhal, Phys. Lett. A **271**, 319 (2000).
  - [14] M. Lewenstein, B. Kraus, J. I. Cirac, and P. Horodecki, Phys. Rev. A **62**, 052310 (2000), URL <http://link.aps.org/doi/10.1103/PhysRevA.62.052310>.
  - [15] O. Gühne and G. Tóth, Physics Reports **474**, 1 (2009).
  - [16] H. Häsele and N. Lütkenhaus, Phys. Rev. A **80**, 042304 (2009), URL <http://link.aps.org/doi/10.1103/PhysRevA.80.042304>.
  - [17] H. Häsele and N. Lütkenhaus, Phys. Rev. A **81**, 060306 (2010), URL <http://link.aps.org/doi/10.1103/PhysRevA.81.060306>.
  - [18] N. Killoran and N. Lütkenhaus, Phys. Rev. A **83**, 052320 (2011), URL <http://link.aps.org/doi/10.1103/PhysRevA.83.052320>.
  - [19] N. Killoran, M. Hosseini, B. C. Buchler, P. K. Lam, and N. Lütkenhaus, Phys. Rev. A **86**, 022331 (2012), URL <http://link.aps.org/doi/10.1103/PhysRevA.86.022331>.
  - [20] I. Khan, C. Wittmann, N. Jain, N. Killoran, N. Lütkenhaus, C. Marquardt, and G. Leuchs, Phys. Rev. A **88**, 010302 (2013), URL <http://link.aps.org/doi/10.1103/PhysRevA.88.010302>.

- [21] Y. Zhao, C.-H. F. Fung, B. Qi, C. Chen, and H.-K. Lo, *Phys. Rev. A* **78**, 042333 (2008), URL <http://link.aps.org/doi/10.1103/PhysRevA.78.042333>.
- [22] I. Gerhardt, Q. Liu, A. I. Lamas-Linares, J. Skaar, C. Kurtsiefer, and V. Makarov, *Nat. Commun.* **2**, 349 (2011).
- [23] C. H. Bennett and G. Brassard, In *Proceedings of IEEE International Conference on Computers, Systems, and Signal Processing* pp. 175–179 (1984).
- [24] C.-H. F. Fung, K. Tamaki, B. Qi, H.-K. Lo, and X. Ma, *Quantum Inf. Comput.* **9**, 131 (2009).
- [25] C. H. Bennett, G. Brassard, and N. D. Mermin, *Phys. Rev. Lett.* **68**, 557 (1992), URL <http://link.aps.org/doi/10.1103/PhysRevLett.68.557>.
- [26] S. Sajeed, P. Chaiwongkhot, J.-P. Bourgoin, T. Jennewein, N. Lütkenhaus, and V. Makarov, *Phys. Rev. A* **91**, 062301 (2015).
- [27] M. Rau, T. Vogl, G. Corrielli, G. Vest, L. Fuchs, S. Nauerth, and H. Weinfurter, *IEEE J. Quantum Electron.* **21**, 1 (2014).
- [28] N. J. Beaudry, T. Moroder, and N. Lütkenhaus, *Phys. Rev. Lett.* **101**, 093601 (2008).
- [29] T. Tsurumaru and K. Tamaki, *Phys. Rev. A* **78**, 032302 (2008), URL <http://link.aps.org/doi/10.1103/PhysRevA.78.032302>.
- [30] J. Löfberg (2004), in *Proceedings of the CACSD Conference*, Taipei, Taiwan.
- [31] T. Moroder, O. Gühne, N. Beaudry, M. Piani, and N. Lütkenhaus, *Phys. Rev. A* **81**, 052342 (2010), URL <http://link.aps.org/doi/10.1103/PhysRevA.81.052342>.
- [32] O. Gittsovich, N. J. Beaudry, V. Narasimhachar, R. R. Alvarez, T. Moroder, and N. Lütkenhaus, *Phys. Rev. A* **89**, 012325 (2014).
- [33] N. Gisin, G. Ribordy, W. Tittel, and H. Zbinden, *Rev. Mod. Phys.* **74**, 145 (2002), URL <http://link.aps.org/doi/10.1103/RevModPhys.74.145>.
- [34] The method using Bell inequalities is an exception. It can be applied to the general case where the detectors involved have arbitrary different efficiencies. Unfortunately, violations of Bell inequalities are usually not robust against transmission loss which is more severe than detection inefficiency in practice. As a consequence, they cannot verify entanglement in many QKD setups.
- [35] Strictly speaking, Eq. (2) defines only EVMs with a bipartite structure, which will be used for verifying entanglement shared between Alice and Bob.